Responses to Reviewer 1's comments

We thank the reviewer for providing valuable comments. We have improved our manuscript following his/her suggestions and comments. Please find our responses below. Reviewer's comments are highlight in blue.

Major comments:

C1) Evaluate vertical profiles of O_3, NO_X, NO_Z from field campaigns.

Figure R1 shows the average vertical profiles of O_3, NO_X, HNO_3 (top panels) and their root-mean-square-error (RMSE) from SEAC^{4}RS campaign. NO_Z species except for HNO_3 are not saved in the WRF outputs along the flight tracks (at 1-min time intervals), and thus only HNO_3 is compared here. The modeled vertical profiles of O_3, NO_X, and HNO_3 are in a reasonable agreement with observations. The large deviations in O_3 near the surface were also reported in previous studies such as Travis et al. (2016). The campaign average differences in vertical profiles of O_3 between CNTR and GOES simulations are small as the aircraft measurements are mostly made in rural environments or high altitudes where O_3 precursor concentrations are low. As shown in the manuscript, the effects of cloud correction are larger under high-NO_X environments than low-NO_X environments. However, it is seen that the cloud corrections slightly reduce O_3 RMSE in general particularly below ~1 km altitude. Some examples from SEAC^{4}RS and NOMADSS flights show that the effects of cloud correction can be considerable if the aircraft flew over relatively high-NO_X regions under cloudy conditions (please see Figs. P3 and P4 in the responses to Dr. Kasibhatla's comments). Even though clouds were present during some flights, the cases allowing to estimate their effects are sparse as aircrafts usually avoid flying on heavily cloudy days. So, when all the data are averaged, the effects of cloud correction are expected to be small. The average profiles and RMSE of NO_X and HNO_3 from CNTR and GOES simulations are also very similar to each other.

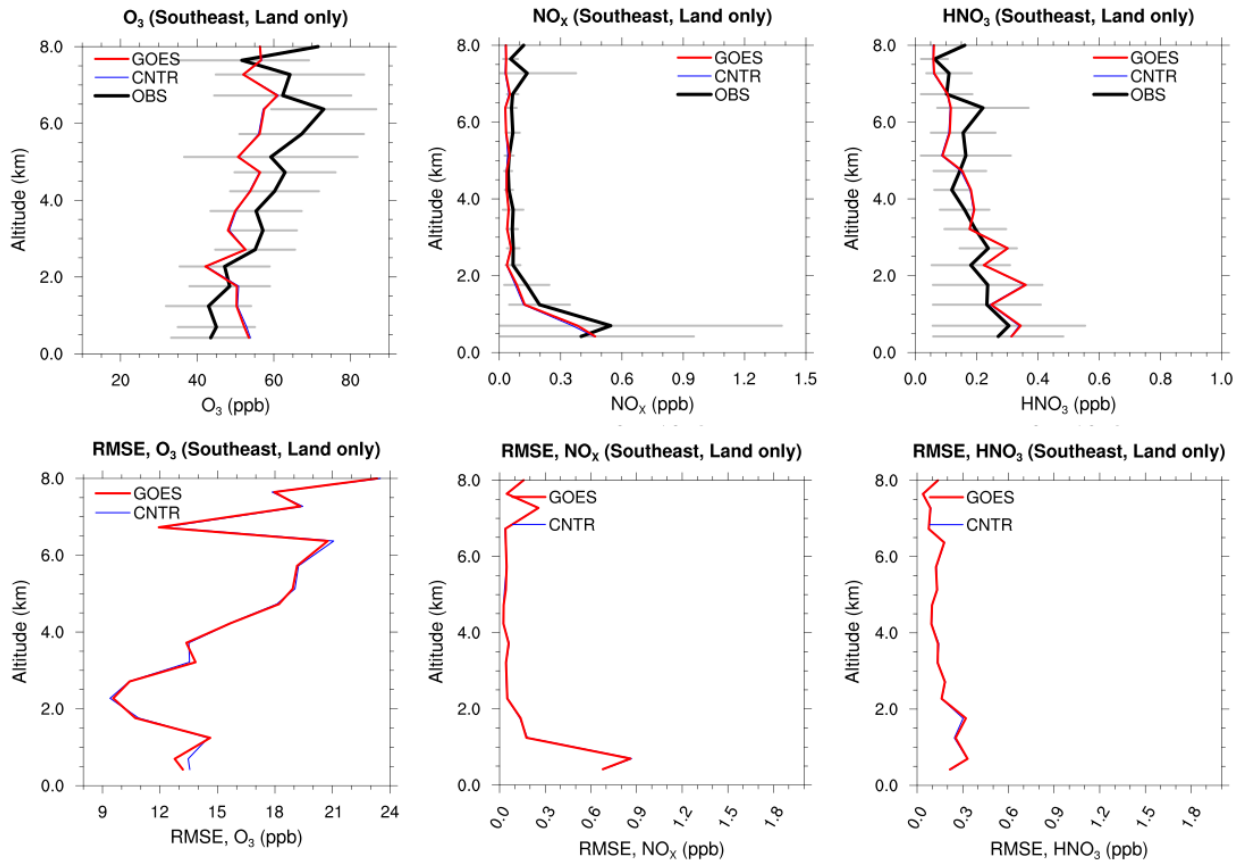

Fig. R1. (Top, from left to right) Averaged vertical profiles of O_3, NO_X, and HNO_3, respectively, for SEAC^{4}RS measurements. The aircraft data over land within the southeast region (latitude: 25–40°N, longitude: 95–70°W) are only used for the averages. (Bottom, from left to right) The corresponding root-mean-square-error (RMSE) of O_3, NO_X, and HNO_3, respectively.

C2) I have some reservations concerning the analyses involving NOx and VOC limited regimes in Sections 5.4 and 5.5 (although I like the last paragraph in Section 5.5). This manuscript has specific conclusions for VOC and NOx limited regimes. There are urban areas that are NOx limited. I suspect the NOx limited conclusions are heavily weighted toward rural areas and don't accurately represent polluted urban and suburban areas. I suggest binning sites based on ozone concentrations and then performing the analyses described in Sections 5.4 and 5.5 so the reader can compare VOC and NOx limited sites with similar ozone concentrations as well as VOC limited sites over a range of ozone concentrations and NOx limited sites over a range of ozone concentrations. Perhaps this can be done by binning the sites based on the peak maximum 8 hour average ozone concentration throughout the year (i.e., bin 1: peak MDA8>75, bin 2: peak MDAO3 between 70-75, …). It may be interesting to include the sites that fall into the transitional zone in your analysis. Include a figure showing delta O3 / delta NOy to identify NOx and VOC limited regimes.

Thanks for providing these valuable suggestions. We agree that analyses for the VOC- and NO_X-limited sites that have similar ranges of O_3 concentration would provide more fair comparisons. Therefore, we performed additional analyses of the sensitivity of maximum daily 8-h average (MDA8) O_3 bias to cloud correction in VOC- and NO_X-limited regimes that have similar peak MDA8 O_3 values. As O_3 concentration is high in summertime, we only consider the period of June through September 2013. All the EPA sites are sorted into several bins based on peak (maximum) MDA8 O_3 concentration during the period of June–September 2013. Figure R2 shows the same analysis as done in Fig. 7 but for various MDA8 bins. Please note that the COD threshold of 30 is not shown here because the number of data with this threshold is too small (generally less than ~50) when the sites are grouped into bins. It is clearly seen that the effects of cloud correction on reducing O_3 bias are greater in VOC-limited regimes than NO_X-limited regimes for all the bins although the degree is somewhat different among the bins. For the NO_X-limited sites that have peak MDA8 O_3 > 75 ppb, the maximum decrease in O_3 bias due to cloud correction is ~3.5 ppb and this value is similar to that (~3 ppb) found in the analysis for all the sites (Fig. 7d in the manuscript). The NO_X-limited sites with peak MDA8 O_3 > 75 ppb are mostly located near the major US cities or the state of California (Fig. R3). Those sites are likely characterized by polluted urban or suburban areas. For the NO_X-limited sites with peak MDA8 O_3 of 60–65 ppb that are mostly located in rural environments, for example, the effects of cloud correction on reducing O_3 bias (maximum value of ~2 ppb) are smaller than those seen for the sites with peak MDA8 O_3 > 70 ppb (maximum value of ~4 ppb). So, even for NO_X-limited regimes it can be said that the effects of cloud correction are larger in more polluted areas. Still, however, the effects of cloud correction are larger in VOC-limited regimes than NO_X-limited regimes. Therefore, our conclusions originally drawn in the manuscript remain unchanged. We mentioned the results of this analysis in the manuscript as follows.

"*We performed additional analysis by dividing VOC- and NO_X-limited sites into groups that have similar ranges of peak MDA8 O_3 concentration during the period of June–September 2013 (Fig. S3). All sites are grouped into bins with peak value of MDA8 O_3 ranging from larger than 75 ppb, 70–75 ppb, 65–70 ppb, 60–65 ppb, to smaller than 60 ppb. The maximum reduction in O_3 bias due to cloud corrections is obtained for the VOC-limited sites with peak MDA8 O_3 of 65–70 ppb and reaches ~8 ppb. The maximum reduction for NO_X-limited sites, on the other hand, is ~4 ppb and is found for the sites with peak MDA8 O_3 of 70–75 ppb. Although the* degree *of the O_3 bias reduction varies somewhat among the bins for a given ozone regime, the effects of cloud correction on O_3 bias reduction remain larger in VOC-limited regimes than NO_X-limited regimes*."

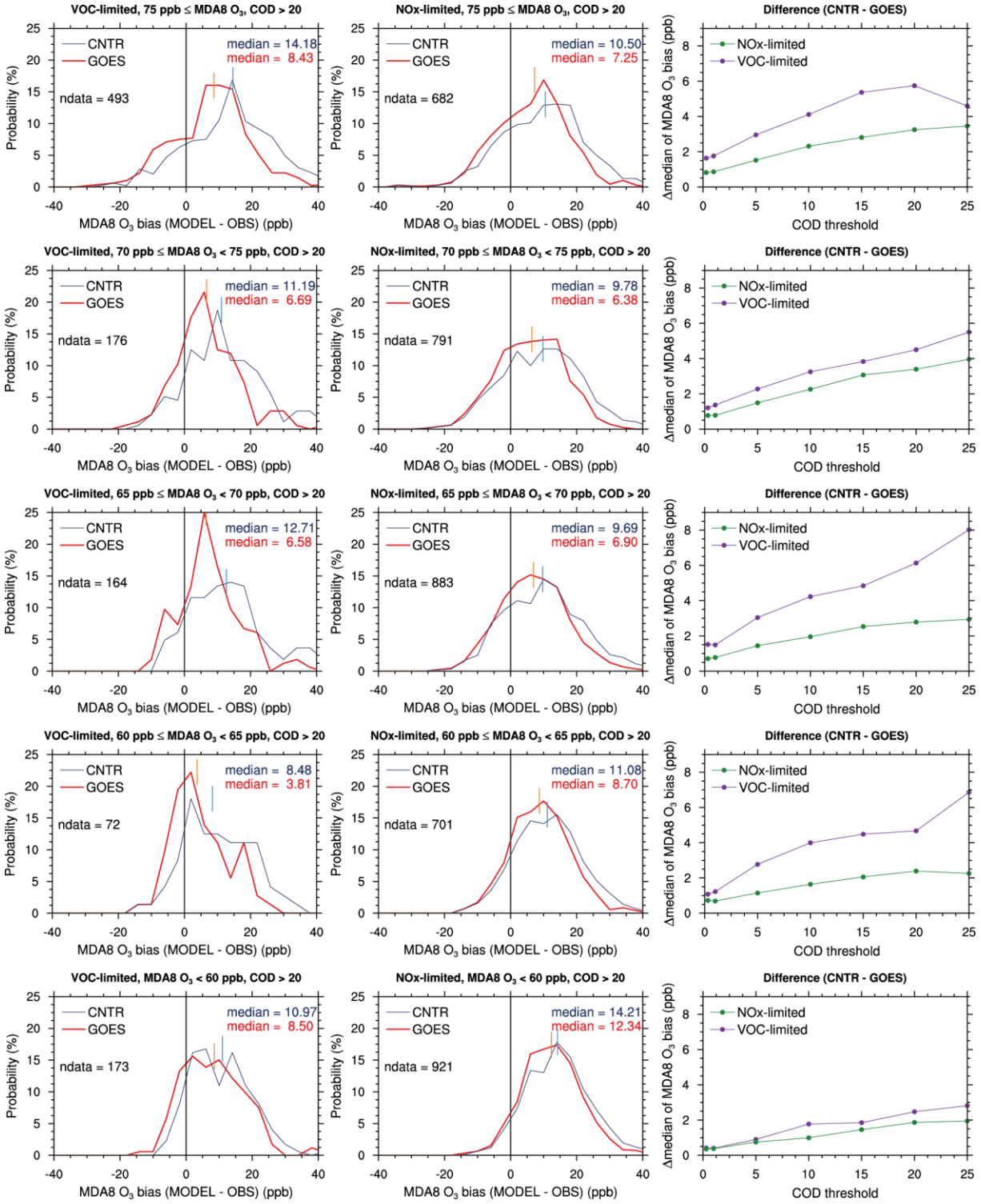

Fig. R2. Similar to Fig. 7 in the revised manuscript but for several bins with different peak MDA8 O_3 ranges.

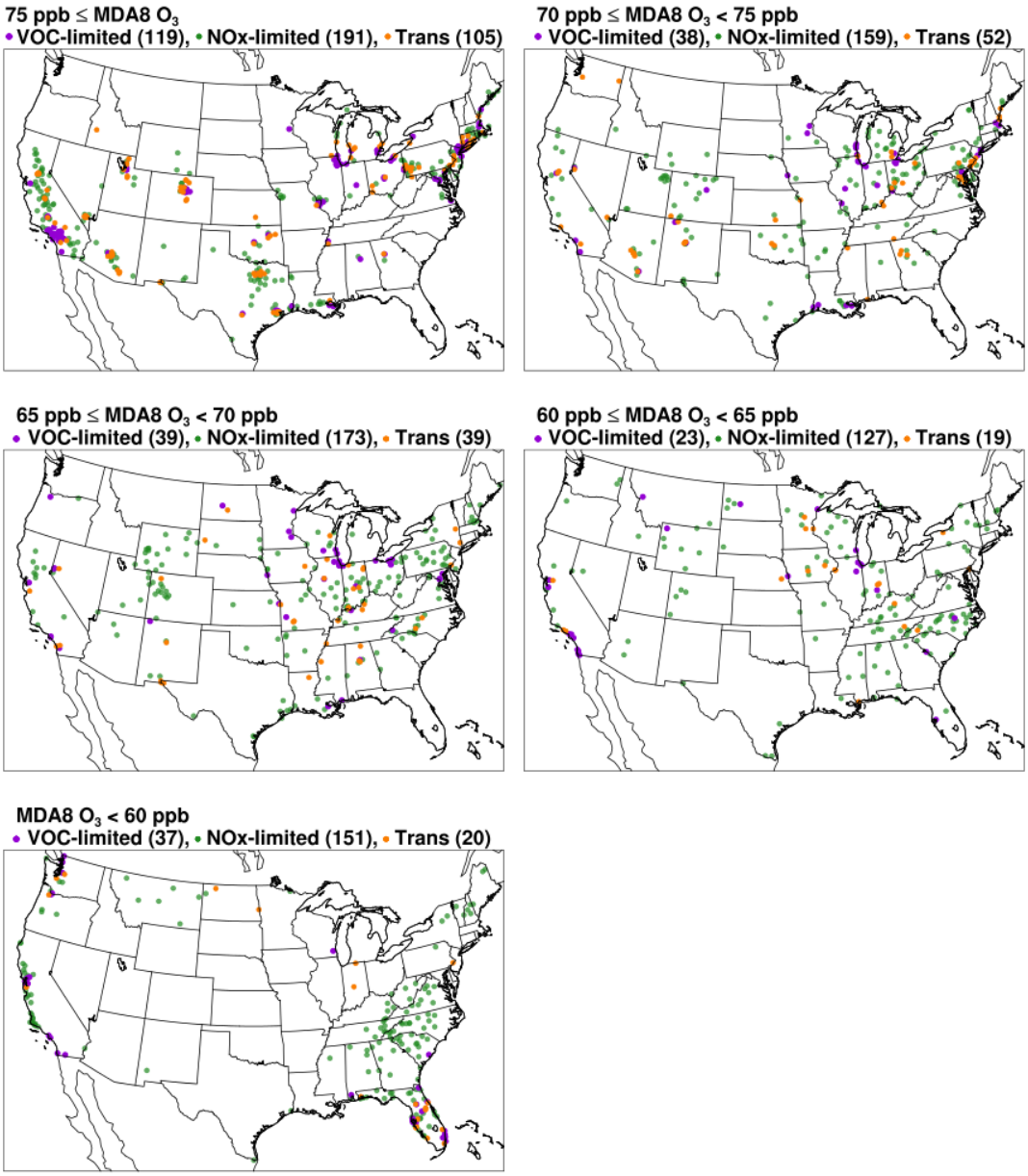

Fig. R3. Maps showing the sites that belong to each peak MDA8 O_3 bin. The number in parenthesis indicate the number of sites in each ozone range. For example, the number of VOC-limited sites with peak MDA8 O_3 > 75 ppb is 119.

In addition, the sites that fall into the transitional zone are added in the analysis (Fig. R4). The effects of cloud correction on O_3 bias reduction for the transition sites are in-between those for the VOC-limited regimes and NO_X-limited regimes. This is now explained in the revised manuscript.

"*Note that the results for the sites in transitional zone (the slope of $\Delta O_3/\Delta NO_y$ is 4–6) showed that the effects of cloud in the transitional zone are intermediate; that is, larger than those for NO_X-limited regimes but smaller than those for VOC-limited regimes (not shown).*"

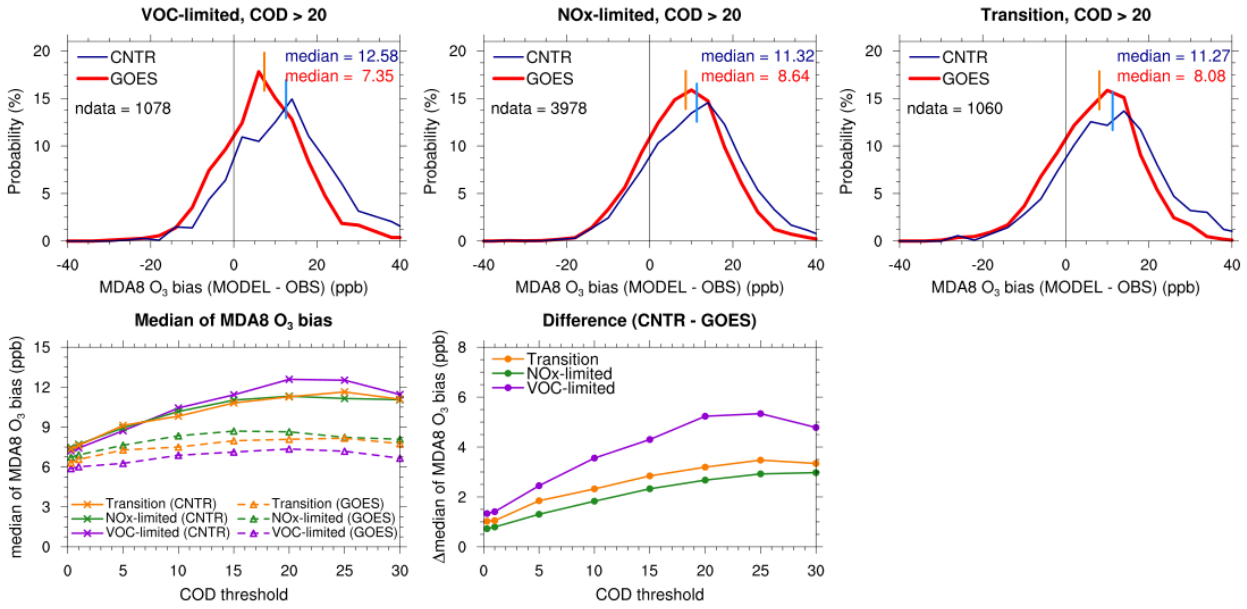

Fig. R4. Same as in Fig. 7 but with the results for transitional zone.

Examples of scatter plots of O_3 and NO_y, which are used to identify VOC- or NO_X-limited sites, are shown in Fig. R5 and following the reviewer's comment we included this in the supplementary material (Fig. S1).

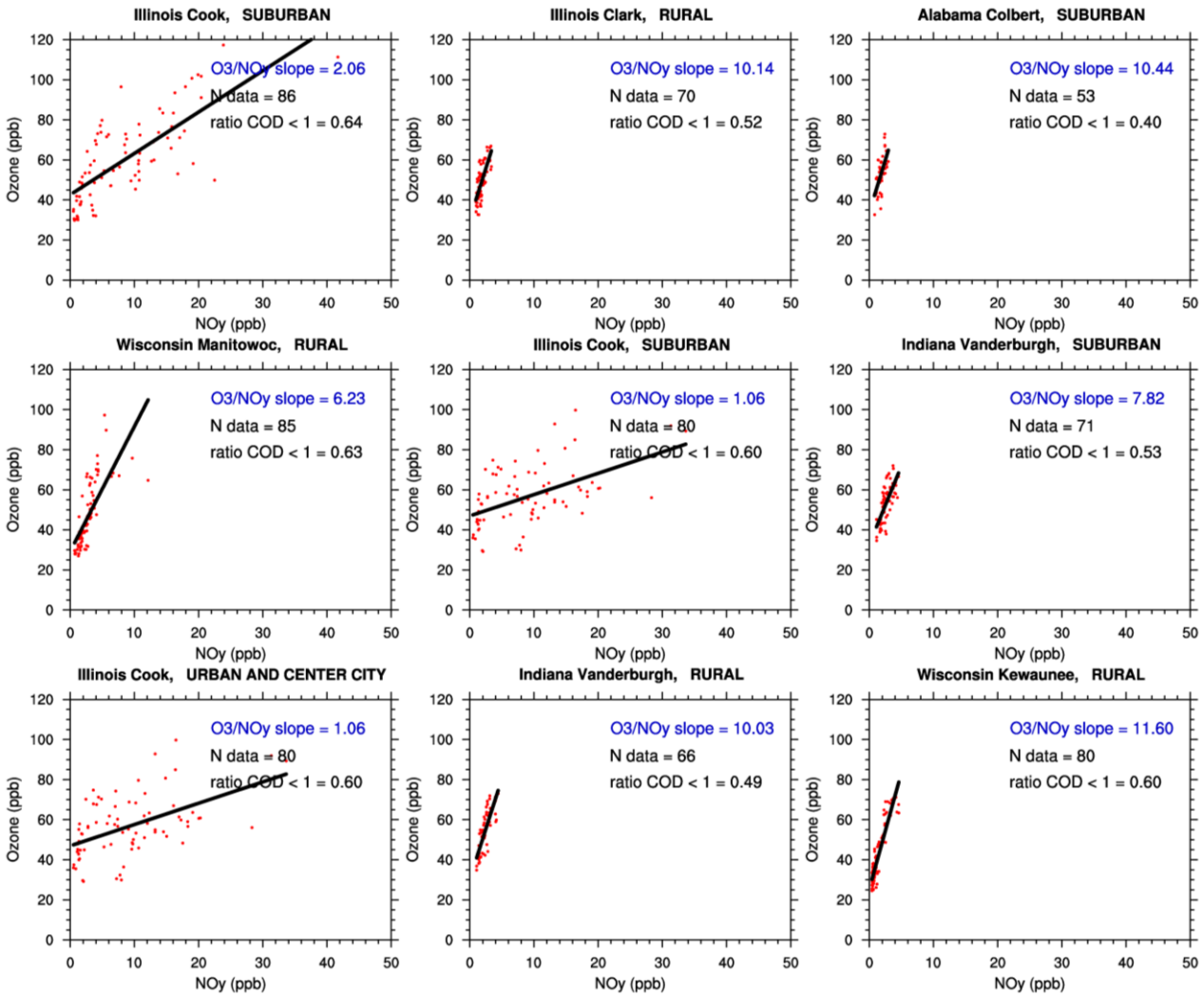

Fig. R5. Scatter plots of O_3 and NO_y. The thick black line indicates the linear regression coefficient. The modeled O_3 and NO_y concentrations at 15–16 local time under clear sky conditions (hourly COD < 1) in the CNTR simulation are used for analysis. On the title heading, the first and second words indicate the state and the county of the site. The third one indicates the type of the site defined by EPA.

Minor comments:

C3) Abstract, line26: Remove mention of "robust with respect to the choice of the microphysics scheme." Only 2 microphysics schemes were tested.

We have removed that part following the reviewer's comment.

C4) Page 5, lines 89-91: Why skip pixels to create an 8km product? Why not leave the product at 4 km?

The 8-km products are sampled every other pixel (4-km pixel) to save processing time. It does not affect the statistics of the analysis.

C5) Page 9, line 181: Change "and with fire" to "and fire"
It is changed.

C6) Page 10, line 189: Change "(Sillman and He (2002)" to "Sillman and He (2002)"
It is corrected.

C7) Page 11, lines 203-204: Change "wrong clouds (that are not present in reality)" to "clouds that are not present in reality"
It is changed.

C8) Page 11, lines 204-205: Re-word this sentence.
It is revised as follows.
"*The overall bias, (A+B)/(A+C), is 0.789 and this means that the WRF underestimates the frequency of cloudy skies.*"

C9) Page 11, line 207: change "except for the mountain regions and northwestern US" to "except for parts of the Rocky Mountains and the Pacific Northwest."
It is changed.

C10) Page 11, line 208: Change "in the central" to "in central"
It is changed.

C11) Page 13, lines 252-253: Change "This is" to "These reductions are". Provide a further explanation of this claim.
It is changed following the reviewer's suggestion. This claim was based on the histograms separating the cloud conditions into below, above, and inside cloud conditions (Fig. R6), which are not shown in the manuscript. The reductions of larger errors with model-to-observation ratio of greater than 2 are due to the reductions under below- and inside-cloud conditions. We elaborate the reasons in the revised manuscript as follows.
"*This is because the number of data influenced by considerably thick clouds is larger in SEAC^{4}RS than in NOMADSS and the measurements in the presence of those thick clouds were mostly made under below-cloud or inside-cloud conditions.*"

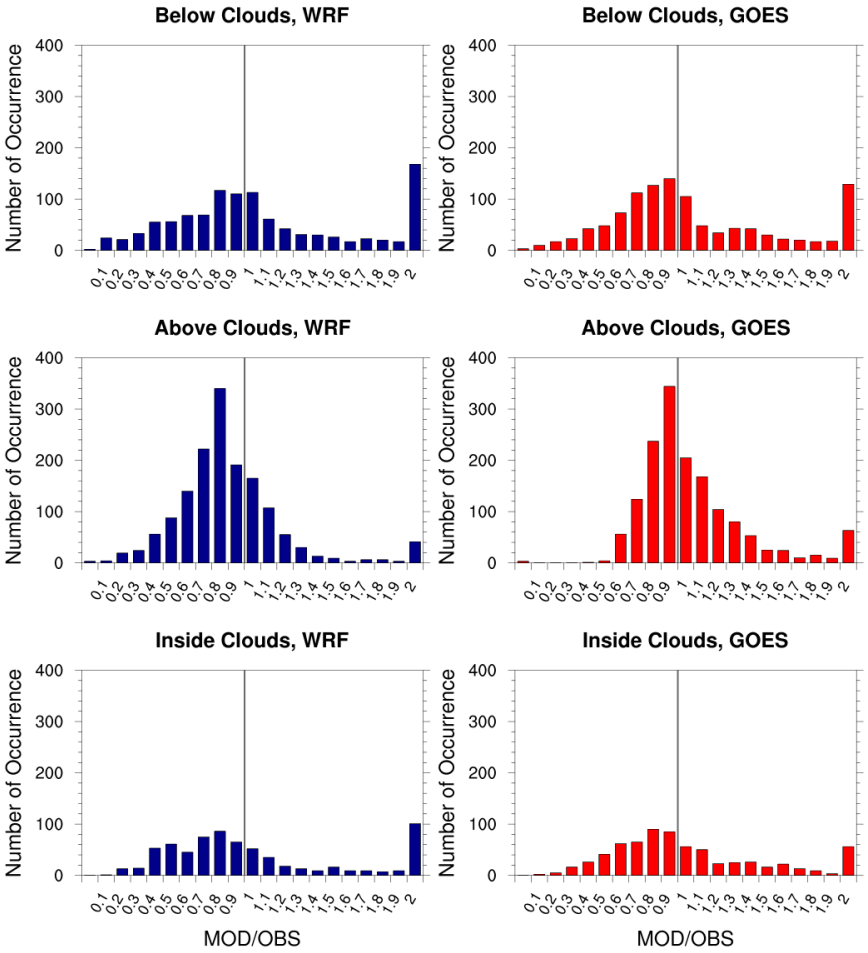

Fig. R6. Histogram of model-to-observation JNO_2 ratio for SEAC4RS under (top) below, (middle) above, and (bottom) inside cloud conditions.

C12) Page 13, lines 254-260: This text states that NOMADSS has a larger mean model-to-observation ratio than SEAC4RS. This is not the case based on Figure 3.

The text was intended to indicate the above cloud conditions. As Fig. R7 shows, the performance in the GOES simulation is not greatly improved even though the satellite clouds are used. The effects of cloud correction for above-cloud conditions for NOMADSS are different from those for SEAC^{4}RS (Fig. R6 middle row). Given that the histograms of Fig. R7 are not included in the manuscript, we have deleted this part in the revised manuscript to avoid confusion.

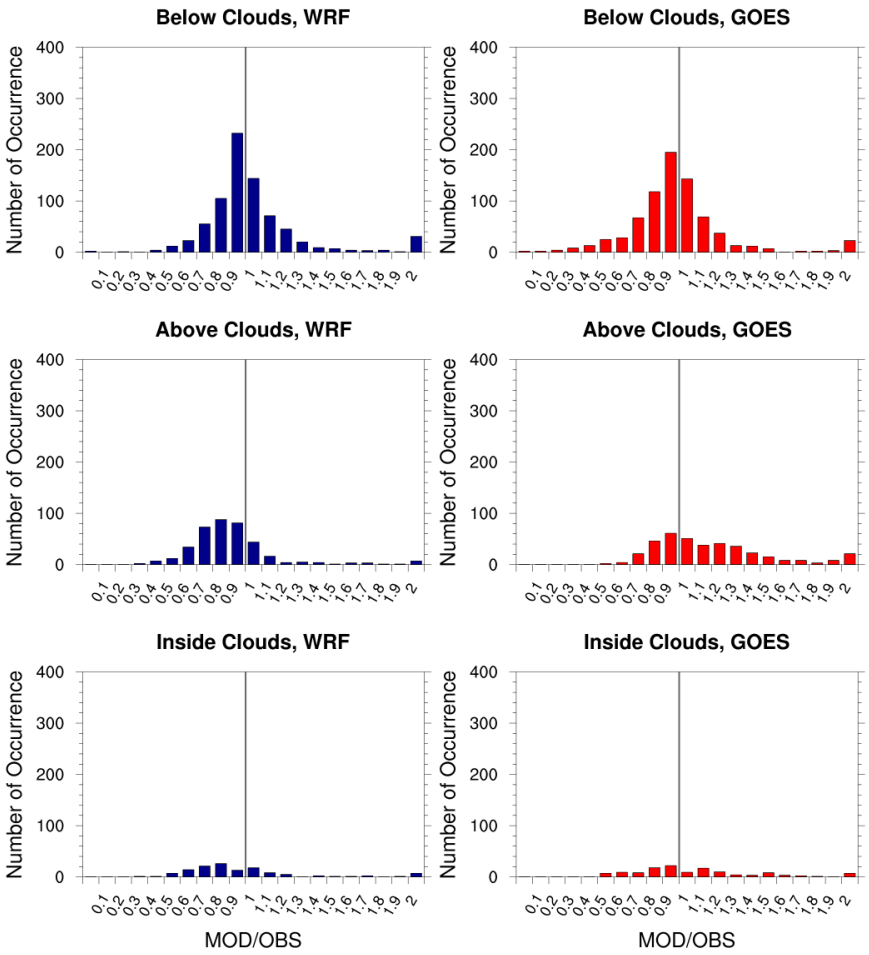

Fig. R7. Histogram of model-to-observation JNO_2 ratio for NOMADSS under (top) below, (middle) above, and (bottom) inside cloud conditions.

C13) Section 5.2: Calculate and discuss model-observations comparison statistics. Use maximum daily 8 hour average O_3 (MDAO3) instead of 8hr average ozone between 10-17 LST.

We have added a discussion of the statistics in the manuscript as requested by the reviewer. Indeed, the root-mean-square-error (RMSE) and correlation coefficient are compared. Both the RMSE and correlation coefficient show a better performance when satellite clouds are used (GOES simulation) than when model clouds are used (CNTR simulation). The RMSE of MDA8 O_3 in the GOES (CNTR) simulation is 13.2 ppb (16.9 ppb) and the correlation coefficient of MDA8 O_3 in the GOES (CNTR) simulation is 0.5 (0.4). This is now explained in the manuscript: *"The performance of the GOES simulation is found to be better than that of the CNTR simulation as compared to observations: for example, under cloudy conditions (COD > 20, see section 5.4 for the criterion), the root-mean-square error of MDA8 O_3 in the GOES (CNTR) simulation is 13.2 ppb (16.9 ppb) and the correlation coefficient of MDA8 O_3 in the GOES (CNTR) simulation is 0.5 (0.4)."*

The spatial ozone distribution map averaged over the study period (Fig. 5) is replaced with MDA8 O_3 in the revised manuscript. The result with MDA8 O_3 is very similar to that shown with daytime 8-h average (10–17 LST) O_3.

C14) Section 5.3: If you have a simulation with "photolysis with WRF clouds and PAR with GOES clouds", this would be interesting to include in this section.

We agree with that. Unfortunately, the current model does not have capability to simulate the setup proposed by the reviewer.

C15) Page 16, lines 316-318 and Figure 6: Difficult to see the relative differences between Figure 6c and 6d. A figure of the absolute value of 6d divided by the absolute value of 6c may be helpful.

Following the reviewer's suggestion, we replaced Fig. 6d with a plot showing the ratio of difference in O_3 between EMIS_BVOC and GOES (previously Fig. 6d) to difference in O_3 between CNTR and GOES (Fig. 6c). The description of this figure is as follows.

"*Figure 6d shows the relative O_3 difference between EMIS_BVOC and GOES simulations to O_3 difference between CNTR and GOES simulations (Fig. 6c).*"

C16) Page 16, lines 318-320: Ozone difference of a simulation with photolysis with WRF clouds and PAR with GOES clouds minus GOES may or may not be 80% of CNTR-GOES. I suggest rewording this sentence to "The contribution of changes in BVOC emissions is ~20% compared to changes of BVOC emissions and photolysis rates using GOES observations."

It is revised based on the reviewer's suggestion:

"*The average contribution of changes in BVOC emissions over land is ~20% compared to changes of BVOC emissions plus photolysis rates using GOES satellite clouds.*"

C17) Figure 4: Use EST or CST, not LST. Map shows areas in the eastern and central time zone.

LST is changed to CST.

C18) Figure 5: Show 3 panels with a CNTR, GOES, and difference plot (CNTR-GOES). Include observations overlayed on-top of the CNTR and GOES plots.

The reason why we show only the result of CNTR simulation is that the spatial distribution of average O_3 in GOES simulation is similar to that in CNTR simulation although the ozone levels are different (Fig. R8). We mentioned the reason why the result of GOES simulation is not shown here in the revised manuscript. In addition, adding observations on the map makes the plot very complicated as the number of sites is ~1300. Lots of sites are closely located to each other as shown in Fig. R3. When all the sites in the bins in Fig. R3 are plotted and overlayed on a map, readers will not be able to see the values of observations.

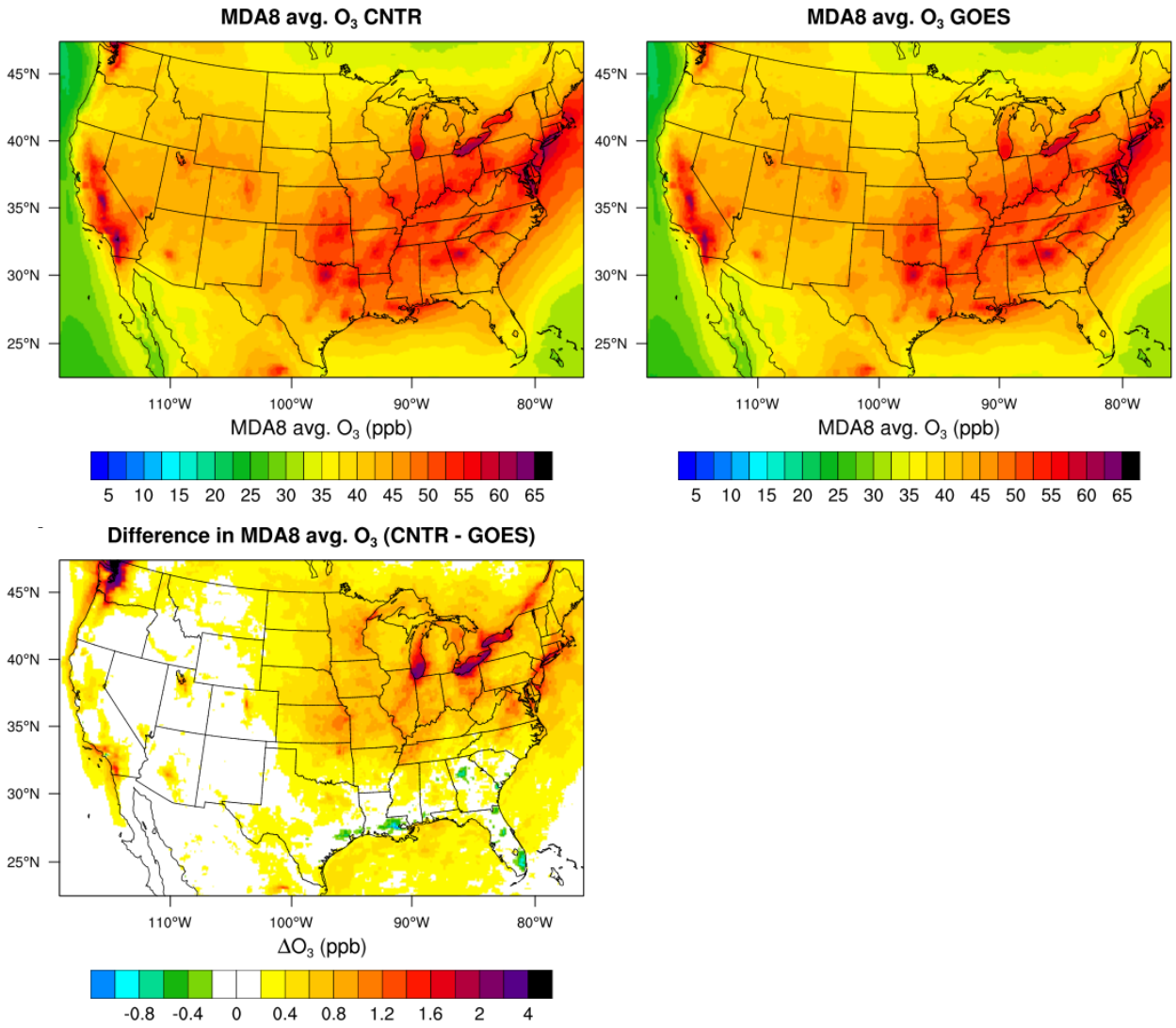

Fig. R8. Spatial distribution of MDA8 O_3 at the lowest model level averaged over the study period (top, left) in the CNTR simulation and (top, right) in the GOES simulation. (Bottom, left) Difference in MDA8 O_3 between CNTR and GOES simulations.

Responses to Reviewer 2's comments

Authors thank the reviewer for providing valuable comments. We have improved our manuscript to address his/her suggestions. Reviewer's comments are highlight in blue, and our responses are in black.

General comments:

C1) The authors mention several times in the manuscript the useful of this technique to improve ozone forecasts. I find this odd, since the technique described uses satellite observed clouds to correct model errors. How would this benefit forecasts? Is the assumption that these satellite data could be assimilated in near real-time, improving the near-term forecast of ozone? Some clarification seems necessary here to explain exactly what the authors have in mind for improving forecasts.

The goal of our study is to quantify the potential benefit of improved cloud fields in air quality modeling. We did not estimate by how much the near real-time ozone forecast could be improved using the observed clouds through data assimilation. This will be done in a future study. The conclusion has been modified to avoid any confusion:

"From the perspective of O_3 forecast, our study indicates that there is a need for an enhanced understanding of the evolution of errors in O_3 forecasts associated with errors in cloud forecasts, and for optimizing the use of meteorological forecasts to allow more accurate near-term O_3 predictions."

C2) I'm also curious about the meteorological performance, although I realize that the cloud assimilation technique only applies to clouds as they affect photolysis. Since WRF tends to underpredict clouds in some regions and overpredict clouds in other regions, does that underprediction/overprediction manifest itself in the meteorological performance (e.g. surface temperature)? If so, this would imply to me that while assimilating clouds to improve photolysis is clearly important, improving clouds in WRF itself, and thereby hopefully improving the overall WRF performance, would be the ultimate goal, since surface temperature (and other meteorological variables), play an important role in not just ozone chemistry but in aerosol chemistry as well. More of thought than something that needs to be addressed in this article.

We thank the reviewer for bringing up these important points. Currently, we corrected cloud fields in WRF using satellite clouds only for radiation that is relevant to photochemistry. So, those cloud corrections do not affect other meteorological variables such as surface temperature, wind, boundary layer height, and so on. The cloud assimilation (cloud analysis more precisely) that has been used in the Rapid Refresh by NOAA (Benjamin et al., 2016), for example, uses satellite cloud products, and in the Rapid Refresh the thermodynamic balance between temperature and humidity due to the presence of clouds is considered, thus affecting temperature

and humidity vertical profiles after cloud assimilation is applied. In addition, the addition or removal of clouds as a result of cloud assimilation affects surface radiation fields (such as downwelling solar radiation) and ultimately surface temperature and wind fields (and others). So, from the perspective of cloud data assimilation, the meteorological variables are all affected by cloud assimilation. We are planning to use the Rapid Refresh forecasts to conduct WRF-Chem simulations in the future and will report how cloud assimilation affects ozone forecasts.

The brief discussion regarding cloud assimilation is added in the last paragraph of conclusions and discussion section as follows.

"The present study corrects cloud fields in WRF using satellite clouds only for radiation that is relevant to photochemistry, and those cloud corrections do not affect other meteorological variables such as surface temperature, wind, humidity, boundary layer height, etc. In a future study, we plan to examine the effects of satellite cloud assimilation on near-term O_3 forecasts using enhanced forecasts such as the Rapid Refresh products from NOAA (Benjamin et al., 2016) that take into account cloud data assimilation to derive meteorology for O_3 forecasts. The Rapid Refresh uses satellite cloud products as well as cloud observations from the ground and considers the thermodynamic balance between temperature and humidity due to the presence of clouds. Thus, this will allow investigating the effects of cloud assimilation on O_3 forecasts not only through changes in radiation for photochemistry but also through changes in meteorological variables."

Specific comments:

C3) Line 14: What is meant by "attributed to that in cloud predictions"?

This was intended to mean "attributed to error in cloud prediction", and we revised it. So, the sentence is as follows.

"It is not well known, however, how much error in O_3 predictions can be directly attributed to error in cloud predictions."

C4) Line 45: Is surface ozone hourly? Perhaps specify if it is.

Yes. It is hourly ozone and we specified this in the revised manuscript.

C5) Line 206: Change "over CONUS" to "over the CONUS".

It is changed.

C6) Line 208: Remove "the" before central California.

It is removed.

C7) Line 211: Change "in supplementary" to "in the supplementary material".

It is changed.

C8) Line 288: I would be a little careful calling this 8-h average O3, since commonly 8-h average O3 refers to calculation of finding the maximum O3 across a number of 8-h averages throughout the day, whereas it appears the authors are simply using an afternoon average consisting of 8 hours. This might cause some confusion to some readers.

Following reviewers' comments, we have all replaced the daytime 8-h O_3 to maximum daily 8-h average (MDA8) O_3 in the revised manuscript.

C9) Line 361: This should be changed to say "partially corrected". It would be presumptions to assume that the cloud fields have been fully corrected. It is a big step in the right direction though.

We here intend to confine the correction to radiation fields relevant to photochemistry. So, the full sentence is revised as follows.

"Still, large O_3 biases of ~11 ppb are present over the southeast US (compared to those of 6–9 ppb over CONUS) even though the clouds and radiation fields that are relevant to photochemistry are corrected."

C10) Line 410: Remove "relatively" before greater.

It is removed.

C11) Fig 5. What is the cause of the very large reduction in O3 over the great lakes in the GOES simulation? Is that due to an improvement in clouds over the lakes themselves, or is it the result of improved clouds over the land and advection of O3 over the lakes? High O3 over the great lakes is a persistent problem in many air quality models, so the resulting improvement warrants some additional discussion in my opinion.

We thank the reviewer for bringing up this point. The correction of clouds both over the lakes and also in the upstream regions (mostly large cities located to the west/southwest of the lakes) can contribute to the reduction in O_3 bias. The precursors are emitted from the upstream cities and both the precursors and O_3 from the cities are advected toward the lakes where O_3 is not readily deposited over the water surface. We found that polluted air masses can be advected over the lakes. In this case in which precursor levels can be high over the lakes, the presence of clouds over the lakes can greatly affect O_3 formation over the lakes.

We added additional discussion in the revised manuscript:

"The example shown here emphasizes the important roles of clouds in the Great Lakes region where large O_3 biases have been reported previously in air quality forecasts (e.g., Cleary et al., 2015). The correction of clouds both over the lakes and in the upstream regions (mostly large cities located to the west/southwest of the lakes) significantly reduces the O_3 bias. It is also shown that polluted air masses from the source regions can be advected over the lakes (not shown). In this case in which precursor levels can be high over the lakes, the presence of clouds over the lakes can greatly affect O_3 formation over the lakes."

Responses to Reviewer 3's comments

Thank you so much for providing valuable comments. We have improved our manuscript following your suggestions and comments. Please find our responses below. Your comments are highlight in blue.

C1) The analysis is based primarily on one set of model physics (Morrison microphysics and Grell 3-D convection). The authors do test the sensitivity of the results to a second microphysics scheme (Thompson) and found little difference. However, the simulation is for summer conditions (June to September), when a significant amount of cloudiness is due to convection. Therefore, there should be a sensitivity test also run with a second convective scheme. I would suggest running the relatively new Grell-Freitas scheme. From what I have seen, this scheme will produce more clouds.

Following reviewer's suggestion, we have performed sensitivity tests with Grell-Freitas scheme. As done for microphysics scheme, a period of 10 days (3–12 July 2013) was considered. An example showing spatial distribution of cloud optical depth from the two cumulus parameterization schemes are presented in Fig. T1. In general, the spatial patterns and the location of large systems are similar to each other. The Grell-Freitas scheme produces more and/or thicker clouds in some regions such as the north Michigan and the south Ohio than the Grell-3D scheme. However, the Grell-Freitas scheme produces fewer and/or thinner clouds in other regions such as the east Texas and North Carolina. In Fig. T2, the histograms of cloud optical depth obtained for the 10-day period from Grell-Freitas scheme (left) and from Grell-3D scheme (right) show that the distributions of cloud optical depth are in general similar to each other. The Grell-Freitas scheme tends to produce fewer clouds with small or moderate cloud optical depth. Figure T3 shows that the degree of cloud correction in reducing O_3 bias is larger in VOC-limited regimes than in NO_X-limited regimes in the simulation with Grell-Freitas scheme, and thus the conclusions originally drawn remain unchanged.

We included the summary of this discussion above in the revised manuscript and figures (Figs. T2 and T3) in the supplementary materials.

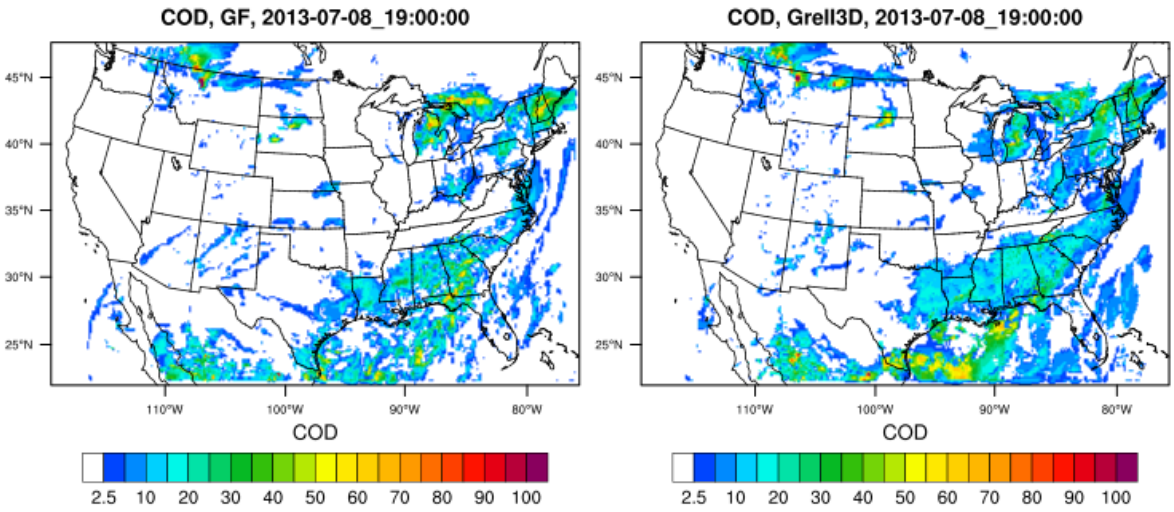

Fig. T1. Cloud optical depth (COD) at 19 UTC 8 July 2013 using the (left) Grell-Freitas scheme and (right) Grell-3D scheme. Both simulations use the Morrison microphysics scheme.

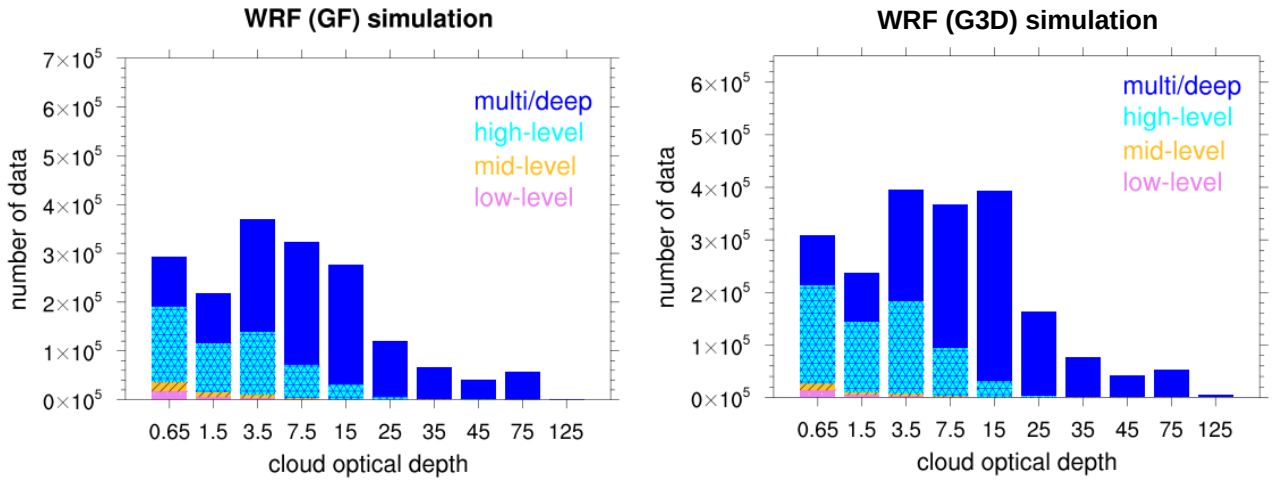

Fig. T2. Histogram of hourly cloud optical depths during the daytime (16–23 UTC) over CONUS (land only) for the period of 3–12 July 2013 from simulations with the (left) Grell-Freitas scheme and (right) Grell-3D scheme.

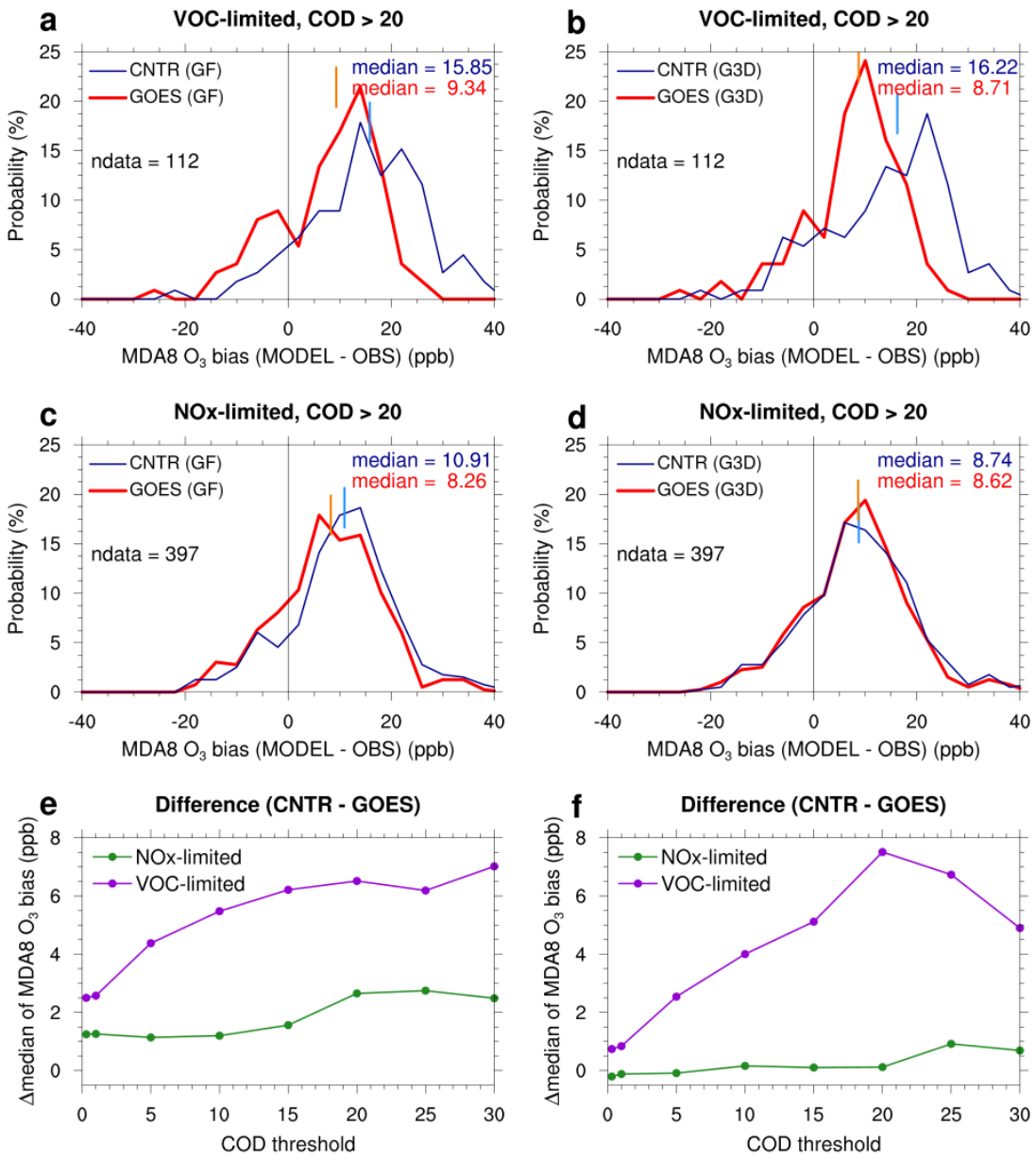

Fig. T3. (Left column) The results of 3–12 July 2013 WRF-Chem simulations with Grell-Freitas scheme. (a/c) Probability density function of MDA8 O_3 bias (model value minus observation value) for VOC/NO_X-limited regime under cloudy sky conditions defined with COD threshold of 20 in the simulations with the Grell-Freitas scheme. (b/d) Same as (a/c), but for the simulations with the Grell-3D scheme. (e and f) Difference in median values of MDA8 O_3 bias between the two simulations with respect to COD threshold (i.e., CNTR minus GOES) for the simulations with the Grell-Freitas and with the Grell-3D schemes, respectively.

C2) In Section 2.3 the authors use the delta O3 to delta NOy ratio to determine VOC-limited and NOx-limited conditions. How is delta NOy determined at EPA monitoring sites? NOy is not

routinely measured at these sites. Even true NOx is measured at only some small fraction of the O3 monitoring sites. This issue needs explanation or substantive revision.

NO_y used in this study is the modeled NO_y and O_3 is also modeled O_3. As you indicated, NO_y is not routinely measured, so the sites having NO_y measurements are very limited. Therefore, we could not rely on NO_y observations. We included the following sentence in the revised manuscript.

"*Note that modeled O_3 and NO_y in the CNTR simulation are used to determine whether an EPA site is in VOC-limited or NO_X-limited regime because NO_y measurements are available for limited sites*."

In addition, we included examples showing how to determine VOC-limited or NO_X-limited sites in the supplementary materials (Fig. S1).

Minor comments:

C3) line 127: Which year NEI NOx was too high? Did Travis et al. indicate all NOx emission types were overestimated, or was it primarily mobile sources?

Travis et al. (2016) used 2011 NEI emissions and adjusted to 2013. They reduced NOx emissions from mobile and industrial sources (all sources except for power plants). Based on the references mentioned in Travis et al. (2016), several local studies reported that NEI NOx emissions for mobile sources are high by a factor of 2 or more (Castellanos et al, 2011; Fujita et al., 2012; Brioude et al., 2013; Anderson et al., 2014).

In our present study, we reduced NO_X emission from all anthropogenic sources by 40% based on the analysis of Travis et al. (2016), and this is mentioned in the revised manuscript.

Reference

Castellanos, P. Marufu, L. T., Doddridge, B. G., Taubman, B. F., Schwab, J. J., Hains, J. C., Ehrman, S. H., and Dickerson, R. R.: Ozone, oxides of nitrogen, and carbon monoxide during pollution events over the eastern United States: An evaluation of emissions and vertical mixing, J. Geophys. Res., 116, D16307, doi:10.1029/2010JD014540, 2011.

Fujita, E. M., Campbell, D. E., Zielinska, B., Chow, J. C., Lind-hjem, C. E., DenBleyker, A., Bishop, G. A., Schuchmann, B. G., Stedman, D. H., and Lawson, D. R.: Comparison of the MOVES2010a, MOBILE6.2, and EMFAC2007 mobile source emission models with on-road traffic tunnel and remote sensing measurements, J. Air Waste Manage., 62, 1134–1149, doi:10.1080/10962247.2012.699016, 2012.

Brioude, J., Angevine, W. M., Ahmadov, R., Kim, S.-W., Evan, S., McKeen, S. A., Hsie, E.-Y., Frost, G. J., Neuman, J. A., Pollack, I. B., Peischl, J., Ryerson, T. B., Holloway, J., Brown, S. S., Nowak, J. B., Roberts, J. M., Wofsy, S. C., Santoni, G. W., Oda, T., and Trainer, M.: Top-down estimate of surface flux in the Los Angeles Basin using a mesoscale inverse modeling technique: as-sessing anthropogenic emissions of CO, NOx and CO2 and their impacts, Atmos. Chem. Phys., 13, 3661–3677, doi:10.5194/acp-13-3661-2013, 2013.

Anderson, D. C., Loughner, C. P., Diskin, G., Weinheimer, A., Canty, T., P., Salawitch, R. J., Worden, H. M., Fried, A., Mikoviny, T., Wisthaler, A., and Dickerson, R. R.: Measured and modeled CO and NOy in DISCOVER-AQ: An evaluation of emissions and chemistry over the eastern US, Atmos. Environ., 96, 78–87, doi:10.1016/j.atmosenv.2014.07.004, 2014.

C4) lines 255 to 260: I don't follow this description of cloud fraction. Please clarify.

This part originally explained the results without showing figures that are relevant to the cloud fraction, but without showing figures we concluded that this part was too confusing to reader, and we decided to remove it. Please see the comment 12 of the first reviewer and our responses.

C5) Section 5.5 describes in detail how the box model calculations show that OH is less sensitive to changes in radiation in the NOx-limited regime. Some statements also need to be made about the effect on P(O3) in the box model.

Figure T4 shows the net chemical production of O_3 in the box model, and the result is consistent with that is found in the WRF-Chem simulations: larger sensitivity of $P(O_3)$ to cloudiness in VOC-limited regimes than NO_X-limited regimes. We briefly included this result in the revised manuscript as follows.

"Note that the net chemical production of O_3 obtained from the box model results also shows a larger sensitivity to cloudiness in VOC-limited regimes than in NO_X-limited regimes (not shown)."

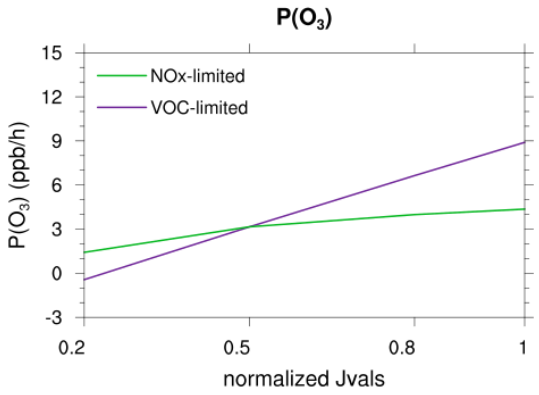

Fig. T4. The net chemical production of O_3 from the box model simulations.

Responses to the comments by Dr. P. Kasibhatla

Thank you for providing valuable comments. Please find our responses (in black) to your comments (in blue) below.

This is an interesting paper that suggests a possible explanation for typical model over-prediction of surface ozone over CONUS (Figure 7). It is not clear however if model simulations are improved both in terms of surface O_3 predictions, as well as O_3 vertical profiles (especially in the boundary layer and just above the boundary layer). While comparisons with measured vertical profiles of JNO_2 are shown in Figure 3, no corresponding comparisons of vertical profiles are shown for O_3. It would be useful to show these comparisons (and provide histograms as is done for JNO_2) with simultaneous aircraft O_3 measurements, especially given the overprediction of JNO_2 in the boundary layer in the GOES simulation compared to the CNTR simulation for the NOMADSS flights (Figure 3).
In terms of model evaluation, it would be also useful to show comparisons of the modeled Ox vs NOz relationship against observations (as is done in Travis et al., 2016) as a check on modeled ozone production efficiency.

1. O_3 vertical profile comparison

The influence of satellite cloud corrections on vertical profile of O_3 is shown in Figs. P1 (SEAC^{4}RS) and P2 (NOMADSS). Only aircraft data over land within the southeast region (latitude: 25–40N, longitude: 95–70W) are used for the averages. Unlike the vertical profiles of JNO_2, which shows considerable improvements when satellite cloud corrections are applied, the vertical profiles of O_3 do not show significant differences between CNTR and GOES simulations even though the histograms of model-to-observation O_3 ratio show slight improvements in the GOES simulation than in the CNTR simulation. This is likely because the aircraft measurements are mostly made in rural environments or high altitudes where O_3 precursor concentrations are low. As shown in the manuscript, the effects of cloud correction are larger under high-NO_X environments than low-NO_X environments. An example on 21 September 2013 shows that GOES simulation better captures the attenuation of JNO_2 under below cloud conditions (~1830–1940 UTC) (Fig. P3). As the aircraft flew over relatively high-NO_X regions during this time period, O_3 concentration shows a better agreement with observations in GOES simulation than CNTR simulation although both the simulations considerably overpredict O_3 in general. The largest difference in O_3 between the two simulations is 5.6 ppb at 1946 UTC. One of the reasons for the overprediction of O_3 could be the overprediction of NO_2 or misplacement of urban plumes. Other example for NOMADSS, on 7 July 2013 when the aircraft flew mostly over the state of Indiana and Lake Michigan shows similar results (Fig. P4). The sky conditions on that day were characterized by broken clouds, and the coarse resolution of satellite data (the original resolution is 8 km at hourly intervals) is another limitation for capturing the exact locations of

small clouds. However, O_3 concentrations along the flight tracks in the two simulations show differences under cloudy conditions and the differences are noticeable only at high NO_2 (e.g., ~1635–1900 UTC). The largest difference in O_3 between the two simulations is 4.4 ppb at 1837 UTC. It should be noted that O_3 concentration in the two simulations is almost the same when NO_2 concentration is low even if JNO_2 values are significantly different (1920–1940 UTC). Thus, even though some cases show that clouds have significant influences on O_3 formation and concentrations above the ground (e.g., within the boundary layer), when all the data points are averaged the effects are hardly noticeable. We anticipate that if airborne measurements of O_3 under cloudy sky conditions are available over cities and/or urban plumes, then we would clearly see the effects of clouds on vertical profiles of O_3. Unfortunately, neither of the campaigns were designed for this purpose, so there are no good airborne observation data to examine the effects of clouds on vertical profiles of O_3.

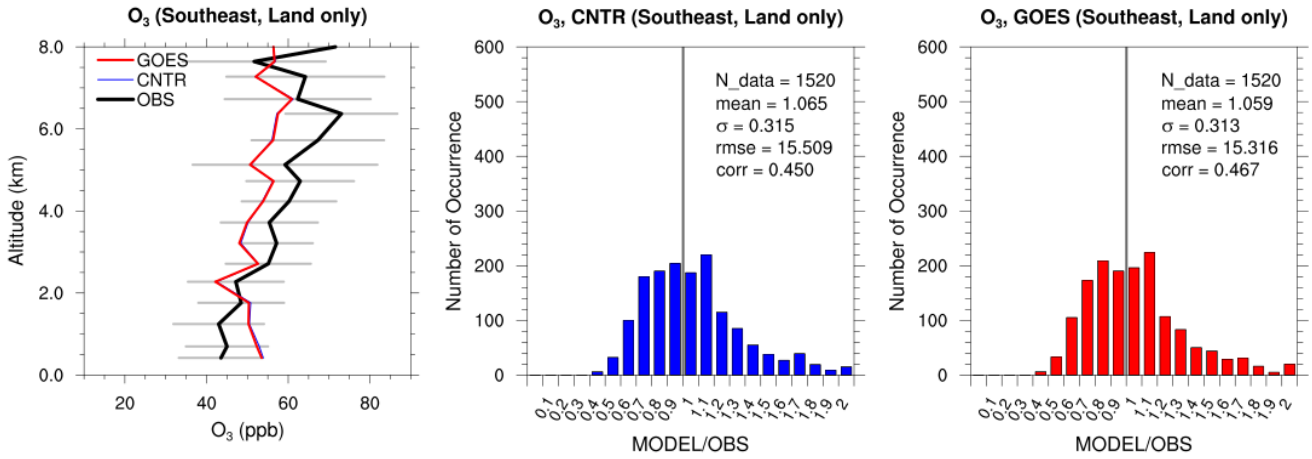

Fig. P1. (Top) (Left) Cloudy-sky averaged vertical profiles of O_3 for SEAC^{4}RS observations, CNTR and GOES simulations. (Middle and Right) Histogram of ratio of O_3 simulated by the model to O_3 observed for CNTR simulation and GOES simulation, respectively.

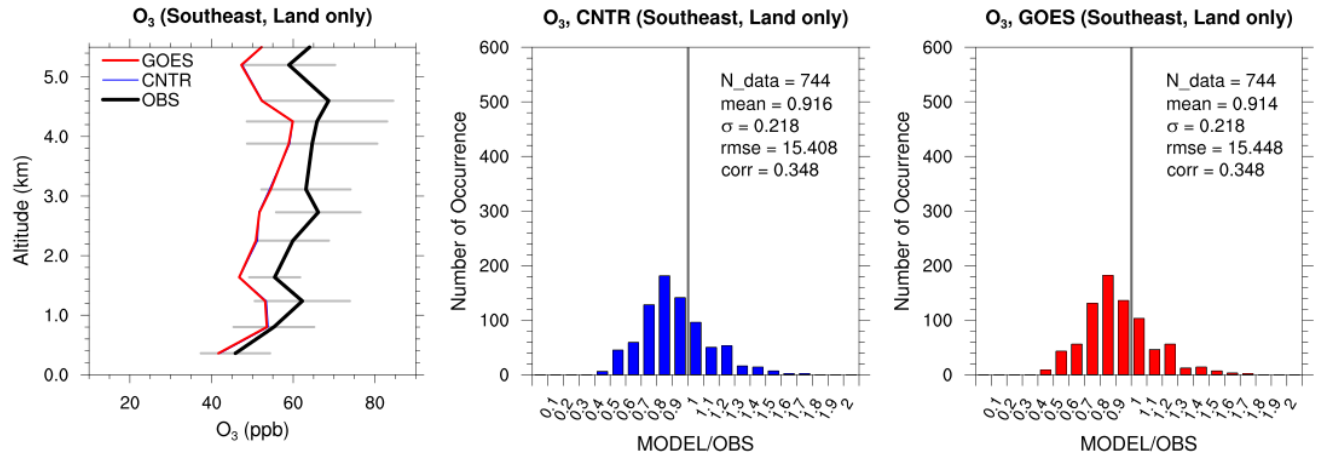

Fig. P2. Same as Fig. P1, but for NOMADSS campaign.

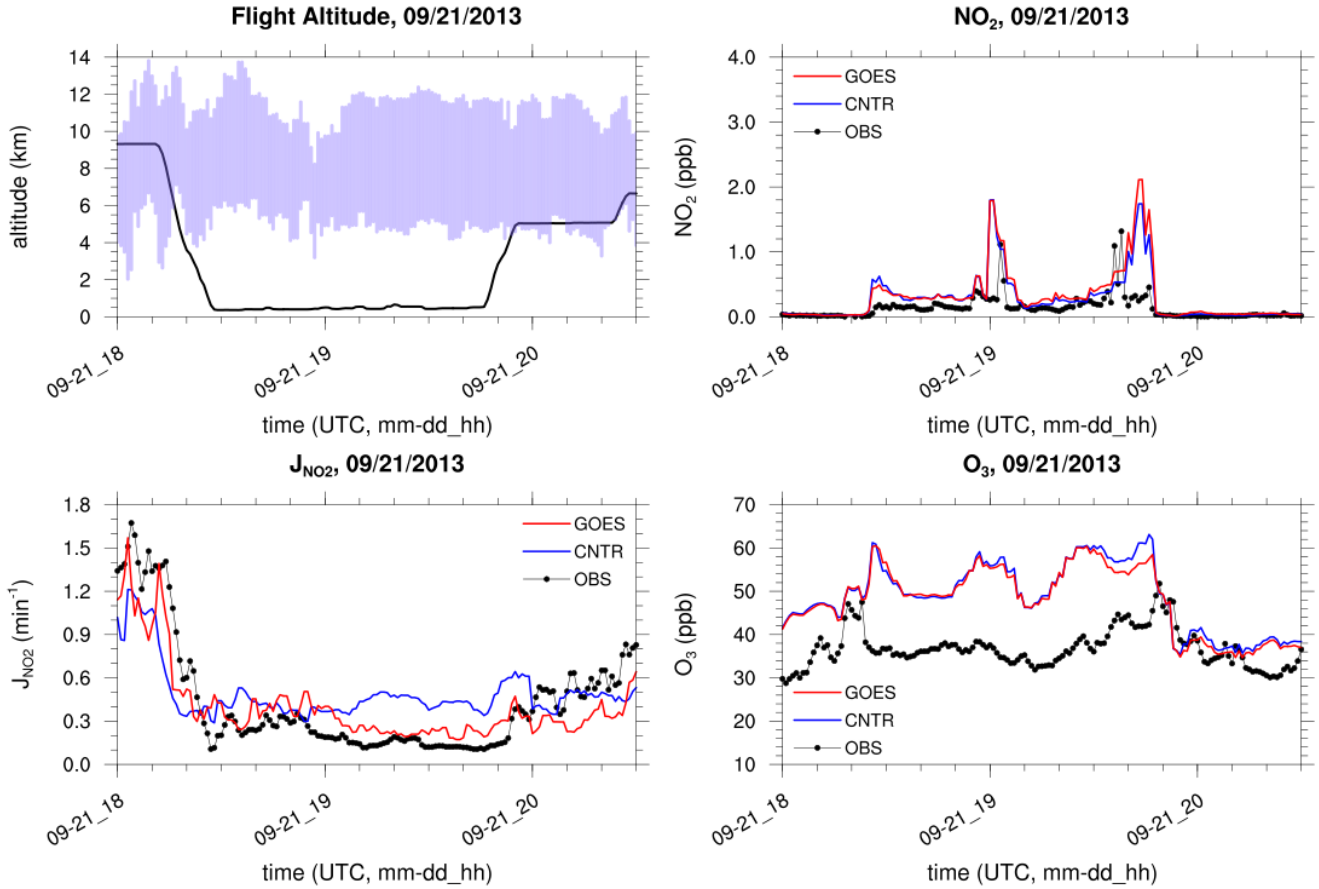

Fig. P3. An example for SEAC^{4}RS campaign (21 September 2013). (Top, left) Timeseries of aircraft altitude. Shading indicates cloud boundaries from GOES retrievals. (Top, right) Timeseries of NO_2 concentration. (Bottom, left) Timeseries of JNO_2. (Bottom, right) Timeseries of O_3 concentration. Note that the shorter time period than the whole flight-day time period is shown here to highlight the effects of clouds.

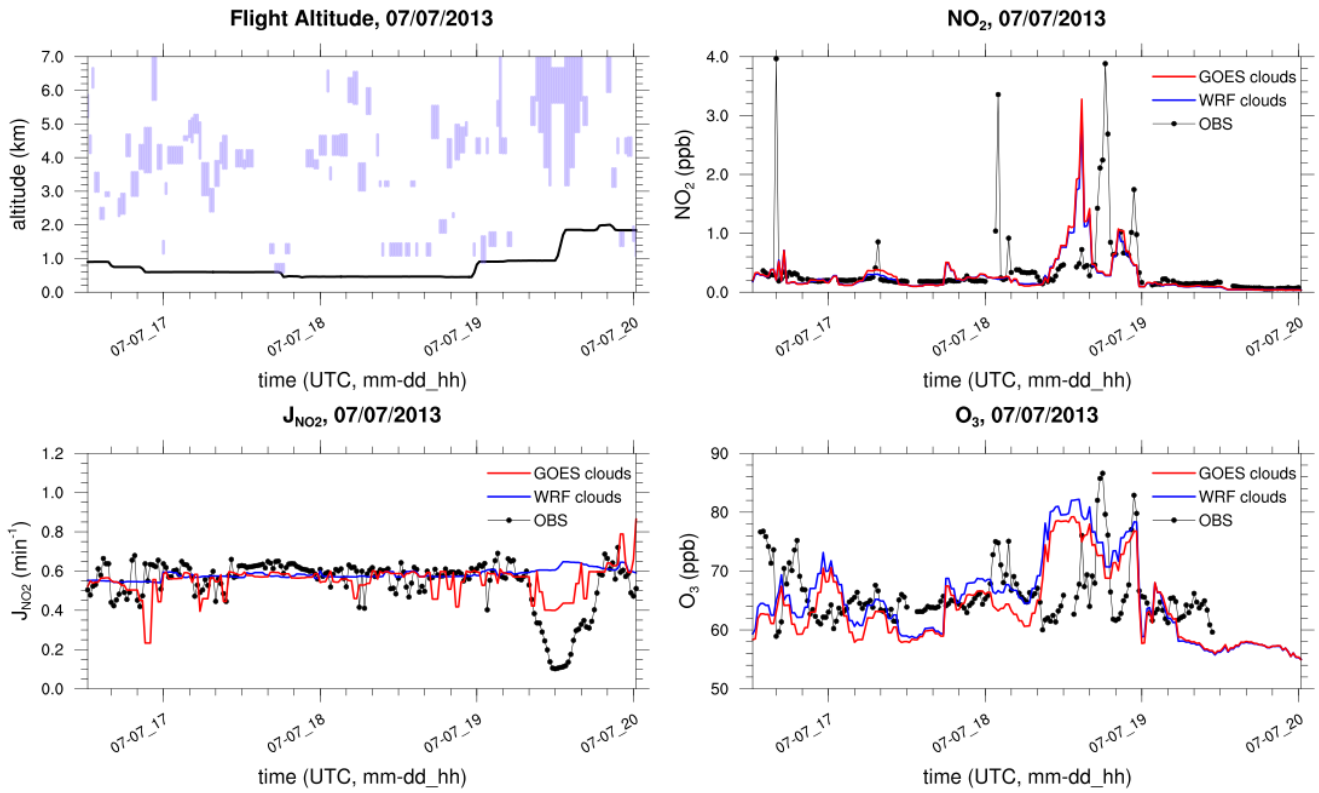

Fig. P4. Same as Fig. P3, but for a NOMADSS example (7 July 2013).

2. Ozone production efficiency evaluation

The ozone production efficiency (OPE) is evaluated against SEAC^{4}RS observations over the southeast US (Fig. P5). The OPE from the model (14.3) is similar to that from the observations (14.0), showing a good performance of our model. Both OPE values are smaller than the values shown in Travis et al. (2016); 16.7 for their model and 17.4 for SEAC^{4}RS observations. Even though we use the same criteria as in Travis et al. (2016) such as altitudes lower than 1.5 km and NO_Z = HNO_3 + PAN + aerosol nitrate + alkyl nitrates, we do not exclude urban plumes and open fire plumes because 1) we are interested in urban areas and urban plumes and 2) the condition of filtering out open fire plumes (using CH_3CN) may not be appropriate to apply to our relatively high resolution simulations. When urban plumes and open file plumes are excluded in the SEAC^{4}RS observations (not shown), we find a very similar value of observed OPE (17.46) as in Travis et al.'s value (17.4).

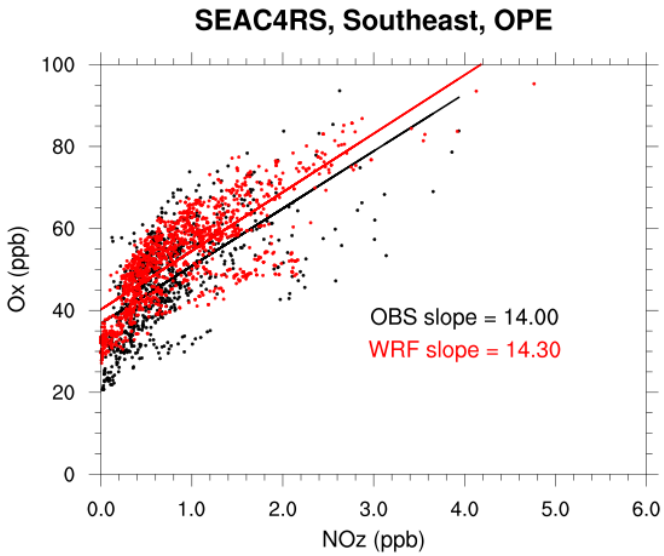

Fig. P5. Ozone production efficiency (OPE) below 1.5 km over the southeast US for SEAC^{4}RS campaign. O_X is O_3 + NO_2, and NO_Z is HNO_3 + PAN + aerosol nitrate + alkyl nitrates.

Quantifying errors in surface ozone predictions associated with clouds over CONUS: A WRF-Chem modeling study using satellite cloud retrievals

Young-Hee Ryu[1], Alma Hodzic[1,2,*], Jerome Barre[1,a], Gael Descombes[1], Patrick Minnis[3]

[1]*National Center for Atmospheric Research, Boulder, CO, USA*

[2]*Laboratoire d'Aérologie, Observatoire Midi-Pyrénées, CNRS, Toulouse, France.*

[3]*NASA Langley Research Center, Hampton, VA, USA*

[a]*now at: European Centre for Medium-Range Weather Forecasts, Reading, United Kingdom*

[1,*]*Correspondence to A. Hodzic: **alma@ucar.edu***

***Key words**: surface ozone, photolysis, satellite clouds, WRF-Chem*

Abstract

Clouds play a key role in radiation and hence O_3 photochemistry by modulating photolysis rates and light-dependent emissions of biogenic volatile organic compounds (BVOCs). It is not well known, however, how much error in O_3 predictions can be directly attributed to ~~that~~error in cloud predictions. This study applies the Weather Research and Forecasting with Chemistry (WRF-Chem) at 12 km horizontal resolution with the Morrison microphysics and Grell 3D cumulus parameterization to quantify uncertainties in summertime surface O_3 predictions associated with the cloudiness over contiguous United States (CONUS). ~~To evaluate the model's own clouds and to restrain the growth of~~All model ~~errors, the model is~~ simulations are driven by reanalysis of atmospheric data and reinitialized every 2 days. In sensitivity simulations, cloud fields used for photochemistry are corrected based on satellite cloud retrievals. The results show that WRF-Chem predicts about 55% of clouds in the right locations and generally underpredicts cloud optical depths. These errors in cloud predictions can lead up to 60 ppb overestimation in hourly surface O_3 concentrations on some days. The average difference in summertime surface O_3 concentrations derived from the modeled clouds and satellite clouds ranges from 1 to ~~6~~5 ppb for ~~the~~maximum daily 8-h average O_3 (MDA8 O_3) over CONUS. This represents up to ~40% of the total ~~8-h average~~MDA8 O_3 bias under cloudy conditions in the tested model version~~, and the results are robust with respect to the choice of the microphysics scheme.~~. Surface O_3 concentrations are sensitive to cloud errors mainly through the calculation of photolysis rates (for ~80%), and to a lesser extent to light-dependent BVOC emissions. The sensitivity of surface O_3 concentrations to satellite-based cloud corrections is about 2 times larger in VOC-limited than NO_X-limited regimes. Our results suggest that the benefits of accurate predictions of cloudiness would be significant in VOC-limited regions which are typical of urban areas.

1. Introduction

Ozone (O_3) is a secondary pollutant that is formed by chemical reactions involving nitrogen oxides (NO_X = NO + NO_2) and volatile organic compounds (VOCs) in the presence of ultraviolet radiation. Because O_3 is a harmful pollutant and a greenhouse gas, there have been numerous efforts aimed at improving O_3 predictions in air quality models, i.e. through a better characterization of the emissions of O_3 precursors (Brioude et al., 2013), more detailed chemical mechanisms (Carter, 2010; Sarwar et al., 2013), more realistic lateral boundary conditions (e.g., Tang et al., 2009), and improved representation of meteorological fields with ensemble modeling techniques (Bei et al., 2010; Zhang et al., 2007). A comprehensive review of the current status and challenges of air quality forecasting is given by Zhang et al. (2012). A large O_3 bias that still persists in most regional and global models is one of the challenges (Brown-Steiner et al., 2015; Fiore et al., 2009; Im et al., 2015; Lin et al., 2017; Travis et al., 2016). The recent multi-model intercomparison study by Im et al. (2015) indicates that over North America models tend to overestimate hourly surface O_3 below 30 ppb by 15–25% and to underestimate O_3 levels above 60 ppb by up to ~80%. It is not quantitatively understood how much the individual processes contribute to O_3 biases. Among meteorological parameters, clouds can be one of the key factors because they greatly modulate the ultraviolet radiation that is critical for O_3 formation. However, they remain one of the largest sources of uncertainties in air quality modeling as Dabberdt et al. (2004) pointed out a decade ago. Accurate cloud predictions in numerical weather models are still challenging, and it has not yet been quantified how much errors in cloud prediction impact surface O_3 predictions.

As satellite cloud products have emerged, providing reasonably accurate data with wide coverage and high temporal resolutions in near-real time (e.g., Minnis et al., 2008), they have been employed in various studies to quantify the effects of clouds on actinic fluxes and/or photolysis rates (Mayer et al., 1998; Ryu et al., 2017; Thiel et al., 2008). Clouds can greatly reduce or enhance actinic flux below, above, and inside clouds, and these effects depend mainly on the cloud optical properties. Ryu et al. (2017) used satellite cloud retrievals of cloud bottom and top heights and cloud optical depth (COD) in a radiative transfer model, and showed that one can obtain fairly good (within ±10%) vertical distributions of cloudy-sky actinic flux using satellite cloud properties. There are, however, only a limited number of studies that have examined the impact of satellite-constrained clouds and photolysis rates on O_3 formation. Pour-Biazar et al. (2007) and Tang et al. (2015) used satellite-observed clouds to correct photolysis rates in a three-dimensional chemistry transport model and reported considerable improvement in surface O_3 simulations. Pour-Biazar et al. (2007) showed that the difference in O_3 due to the errors in cloud predictions can be up to 60 ppb for a given pollution episode over the south US. Tang et al. (2015) showed that 1-month averages of 8-h surface O_3 can differ by 2–3 ppb between the simulations using satellite-derived clouds and model-predicted clouds over the south US. These studies were performed for rather short time periods (a week or a month) over limited areas, and provide motivation for a more systematic/comprehensive quantification of the importance of cloud errors in O_3 predictions in summertime and for various chemical regimes.

In the present study, we use satellite-derived COD and cloud boundaries to constrain radiation fields that impact photochemistry, i.e., photolysis rates and light-dependent BVOC emissions, in a three-dimensional chemistry transport model (WRF-Chem). Our study targets the contiguous United States (CONUS) and numerical simulations are performed for June–September 2013. The

WRF-simulated clouds are first evaluated against the Geostationary Operational Environmental Satellite (GOES) data (section 3). The vertical profiles of NO_2 photolysis rates are evaluated against in-situ airborne measurements during two field campaigns (section 4). The O_3 biases arising from inaccurate cloud predictions are quantified, and discussed in light of the sensitivity of O_3 chemistry to COD (section 5). Unlike the previously mentioned studies, here we quantify separately the contributions of errors arising from changes in photolysis rates altered by clouds vs. those arising from light-dependent BVOC emissions to the O_3 biases. Conclusions and discussion are given in section 6.

2. Methodology

2.1. Satellite retrievals

The GOES retrievals were performed using the Satellite ClOud and Radiation Property Retrieval System (SatCORPS), which is an adaptation of the Minnis et al. (2011) algorithms for application to imagers on all geostationary weather satellites (Minnis et al. 2008) and on NOAA and MetOp satellites (Minnis et al. 2016). For SatCORPS, the algorithms of Minnis et al. (2011) were altered as described by Minnis et al. (2010) using the low-cloud height estimation method of Sun-Mack et al. (2014) and the severely roughened hexagonal column optical model of Yang et al. (2008) for ice cloud COD retrievals. This study uses a subset of the hourly, 8-km SatCORPS cloud retrievals from GOES 13 (GOES-East) and GOES 15 (GOES-West) for the North American domain. The 8-km resolution is achieved by analyzing only every other 4-km pixel and line. Each pixel is considered to be either 100% cloudy or 100% clear. Of the variety of cloud properties available, this study only uses cloud bottom height, cloud top height, and COD. Uncertainties in the cloud products are summarized by Ryu et al. (2017).

Images from coincident times were unavailable for the two satellites: the GOES 13 and GOES 15 data are offset by 15 min. The GOES 13 data taken at UTC + 45 min at every hour were matched with the GOES 15 data at UTC + 00 min. The pixel-level retrievals were re-gridded to a 12-km resolution to match the WRF-Chem domain (see section 2.2) using the Earth System Modeling Framework (ESMF) software and the nearest-neighbor interpolation. Because of the coverage difference between the two satellites, the data of the nearest time from the two satellites (e.g., 1845 UTC from GOES 13 and 1900 UTC from GOES 15) are merged at 105°W, which is equidistant from the two sub-satellite longitudes. Only daytime hours (09–23 UTC and 00–04 UTC) are used here.

2.2. WRF-Chem model simulations

The present study employs the WRF-Chem model version 3.6.1. with the updated photolysis scheme. A single domain is used with a horizontal grid size of 12 km (Fig. 1). The meteorological initial and boundary conditions are provided by the NCEP FNL (Final) Operational Global Analysis data with a horizontal resolution of 1°, which are available every 6 hours. The model is initialized at 00 UTC 1 June 2013 and spun-up for the first 10 days in the control simulation (CNTR simulation). The meteorological fields are re-initialized every 48 hours at 06 UTC of a given day to avoid the growth of model errors, and the model is run for 54 hours. Here, the first 6 hours are allowed for spin-up and discarded in each run. The model outputs for the period of 12 UTC 11 June 2013 through 12 UTC 1 October 2013 are used for the analysis. As the goal of the study is to use and evaluate the modeled clouds and their impact on O_3 predictions, nudging is not used. This is different from many previous air quality studies that nudged the meteorology and evaluated modeled O_3 with observations. The physics options used

are the Morrison two-moment scheme (Morrison et al., 2009) for the microphysics, RRTMG scheme for longwave and shortwave radiation (Iacono et al., 2008), MYNN 2.5 level TKE scheme for the boundary layer parameterization (Nakanishi and Niino, 2006), MYNN surface layer scheme, Noah land surface model (Chen and Dudhia, 2001), and Grell 3D ensemble scheme (Grell and Devenyi, 2002) for cumulus parameterization with radiation feedback. The initial and boundary conditions for chemical species are obtained from the Model for OZone And Related chemical Tracers (MOZART) global simulation of trace gases and aerosols. For each 2-day simulation, the chemical state of the atmosphere at 06 UTC is obtained from that at 06 UTC of the previous simulation. The MOZART-4 mechanism is used for gas-phase chemistry as described in Knote et al. (2014), and the Model for Simulating Aerosol Interaction and Chemistry (MOSAIC) aerosol module with 4 bins is used for the aerosol chemistry. Anthropogenic gas and aerosol emissions are adopted from the AQMEII project in which the emissions were projected to 2010 from the NEI 2008 inventory (Campbell et al., 2015). Since Travis et al. (2016) reported that NEI NO_X emissions are too high, we reduced NO_X emission from all anthropogenic sources by 40% ~~following~~based on their analysis. Note that the NO_X and PAN from the lateral boundaries are also reduced by 40% in our study. Biomass burning emissions are taken from the Fire Inventory from NCAR (FINN) (Wiedinmyer et al., 2011). Model of Emissions of Gases and Aerosols from Nature (MEGAN) (Guenther et al., 2006) version 2.04 is used for BVOC emissions. As done in Travis et al. (2016) to better match isoprene flux observations during the Studies of Emissions and Atmospheric Composition, Clouds and Climate Coupling by Regional Surveys (SEAC^{4}RS) field campaign (Toon et al., 2016), we reduced MEGAN isoprene emissions by 15% over the southeast US. The photolysis rate calculations utilize the newly implemented TUV option in the WRF-Chem model (Hodzic et

al., 2017 in preparation). This new TUV option uses the updated cross section and quantum yield data based on the latest stand-alone TUV model version 5.3, and considers 156 wavelength bins with the resolutions of 1–5 nm. The COD is calculated based on the parameterization given in Chang et al. (1987), which uses cloud liquid water and/or ice water contents and effective droplet radius (assumed to be 10 μm both for liquid and ice droplets). To represent subgrid cloud overlaps, a simple equation of Briegleb (1992) is used, i.e., the effective COD = COD_0 × (cloud fraction)$^{1.5}$, where COD_0 is the cloud optical depth that is calculated following Chang et al. (1987), and the cloud fraction is determined based on the relative humidity in a given grid box. According to Briegleb (1992), applying a power of 1.5 to the cloud fraction is equivalent to the maximum random overlap.

In the present study, we performed two sets of simulations that use WRF generated clouds in the CNTR simulation and the GOES clouds in the GOES simulation. The GOES simulations are conducted from 06 UTC 11 June 2013 through 12 UTC 1 October 2013. The initial chemistry conditions in the GOES simulation are adopted from the outputs of the CNTR simulation at 06 UTC 11 June 2013. The satellite cloud retrievals are used only to correct photolysis rate and photosynthetically active radiation (PAR) calculations (i.e., only within the TUV model in WRF-Chem). That is, the satellite cloud information is not linked to dynamics, microphysics, and atmospheric radiation. The value of COD is linearly distributed through vertical grids from the cloud bottom to the cloud top within the TUV model as done in Ryu et al. (2017). This method is different from the one used in Pour-Biazar et al. (2007) and Tang et al. (2015) in which cloud bottom height used in their photolysis rate calculations is estimated from the meteorological model rather than retrieved from the satellite. The use of model estimates can lead to additional uncertainties in the case of misplaced model clouds compared to observations.

In the present study, PAR calculated from the TUV model is used for the BVOC emissions in MEGAN for all simulations. This is different from the PAR conventionally used in MEGAN, which is simply converted/scaled from the downward shortwave radiation from the atmospheric radiation scheme. In the CNTR (GOES) simulation, the WRF generated clouds (GOES clouds) are used for the PAR calculation within the TUV model.

To examine the impact of changes in BVOC emissions on surface O_3, another set of sensitivity simulation (EMIS_BVOC simulation) is performed for 10 days (3–12 July 2013), which uses WRF-generated clouds for the PAR calculation and BVOC emissions as in the CNTR simulation but uses the GOES clouds for photolysis rate calculations as in the GOES simulation. The description of the control and sensitivity simulations is summarized in Table 1.

2.3. Observational data

2.3.1. Aircraft data from field campaigns

We evaluate the model performance using airborne measurements made during two field campaigns in 2013, i.e., the NOMADSS (Nitrogen, Oxidants, Mercury and Aerosol Distributions, Sources and Sinks) and the SEAC^{4}RS campaigns. The detailed description of the instrument and measurement data is given in Ryu et al (2017). The NOMADSS campaign was conducted during 1 June–15 July 2013 mainly over the southeast US. We use 16 flight-day data at 1-min time intervals for the analysis. Data with solar zenith angles larger than 85° are not used. The fire plume data are filtered out by excluding the data showing NO_2 (> 0.1 ppb) or CO (> 120 ppb) aloft at 4–7 km level. Based on the GOES cloud data, 68% of flight data are characterized by clear skies and the remaining data (32%) had clouds in the vertical column where the airplane

was located. The SEAC^{4}RS campaign also targeted the southeast US although the airplane sometimes flew over a larger region including California and Midwestern US. The period used for the analysis is from 6 August through 23 September 2013, which includes 21 flight days. The time intervals are also 1-min and the data with large solar zenith angles (> 85°) and ~~with~~ fire plumes are filtered out. The fraction of data with clouds is 41% for SEAC^{4}RS. It is noteworthy that SEAC^{4}RS measurements include large and thick clouds in some cases as a few of the campaign goals are to identify the role of deep convection in redistributing pollutants and aerosol-clouds feedbacks, whereas the clouds during NOMADSS were mostly broken clouds.

2.3.2. Ground ozone data

The United States Environmental Protection Agency (EPA) hourly O_3 measurements are used for the analysis. To examine the sensitivity of O_3 to COD in different chemical regimes, the VOC- and NO_X-limited regimes are identified using the ratio of $\Delta O_3/\Delta NO_y$, following Sillman and He (2002). They reported that the NO_X-VOC transition occurs when $\Delta O_3/\Delta NO_y$ = 4–6. Thus, an EPA site is denoted as a VOC-limited (NO_X-limited) regime when the ratio is less than 4 (greater than 6). Examples showing the ratio of $\Delta O_3/\Delta NO_y$ for several sites are given in the supplementary materials (Fig. S1). Among 1,299 EPA sites, 1,062 are used for the analysis: 24% of the sites are in the VOC-limited and 76% in NO_X-limited regimes. The remaining 237 sites are not used in the present study because those sites fall into the transitional zone, i.e., $\Delta O_3/\Delta NO_y$ = 4–6. Note that modeled O_3 and NO_y in the CNTR simulation are used to determine whether an EPA site is in VOC-limited or NO_X-limited regime because NO_y measurements are available for limited sites.

3. Evaluation of WRF clouds with satellite measurements

The model bias in the cloud spatial coverage is evaluated using a 2×2 contingency table (Table 2), where A and D correspond to hit and correct negative events, respectively, and B and C to false alarm and miss events, respectively. Here, a threshold of 0.3 in hourly COD is used to distinguish between clear and cloudy sky as the lowest detection limit of satellite retrieved COD over land is estimated to 0.25 in Rossow and Schiffer (1999), and the use of 0.3 poses slightly stricter conditions for cloudiness. The agreement index, which is defined as A+D (WRF predicts correctly cloudy or clear skies), is 69.7% and the probability of detection (POD) for clouds, A/(A+C), is 55.6%. It is found that the fraction of errors in missing clouds (C, 19.8%) is larger than that of predicting ~~wrong~~ clouds ~~(~~that are not present in reality~~)~~ (B, 10.4%). The overall bias, (A+B)/(A+C), is 0.789 and this means that the WRF underestimates the frequency of cloudy skies~~ as the ratio of (A+B)/(A+C), 0.789, indicates smaller than 1.~~. Figure 1 shows the spatial distribution of each contingency category over the CONUS ~~as~~ averaged over the whole study period. In general, the eastern US shows higher cloud frequencies than the western US except for parts of the ~~mountain regions~~Rocky Mountains and ~~northwestern US.~~the Pacific Northwest. The largest agreement index appears in ~~the~~ central California where the sky condition is mostly clear (Fig. 1d). In terms of errors, the missing clouds rate has its highest frequency (20−35%) in the Midwestern and northwestern US, while the highest frequency of false alarm (20–30%) occurs over the southeast US and the southeastern Texas. The sum of category B and C can be found in the supplementary material (Fig. ~~S1~~S2). It should be noted that the contingency categories are based on binary results of cloud-free or cloudiness and so they do not provide quantitative comparison of cloud optical properties, e.g., COD. For example, even though the WRF model

produces clouds in the right locations (category A), the WRF CODs can differ from those retrieved from satellite data.

Figure 2 evaluates quantitatively COD and vertical extent of clouds between the model and satellite retrievals. The vertical extent of clouds is classified based on the International Satellite Cloud Climatology Project (ISCCP) definition (Rossow and Schiffer, 1999), which are as follows: i) low-level: cloud top height $\leq$ 3 km, ii) mid-level: 3 km < cloud top height $\leq$ 6 km, iii) high-level: cloud bottom height > 6 km, and iv) multi-layered or deep convection: cloud bottom height $\leq$ 6 km and cloud top height > 6 km. Even though multiple cloud layers can be resolved in the WRF model, these kinds of clouds are not resolved in the satellite retrievals used in this study. Thus, for a fair comparison, the multi-layered clouds in the WRF model are not further resolved into cloud layers. Note that the liquid/ice water contents from cumulus clouds (parameterized clouds) are included in the model COD calculations.

The frequency distribution of CODs does not have the same shape in the model and observations. The WRF model overpredicts by a factor of 2 very thin clouds with COD < 1, whereas the GOES retrievals show that the most abundant clouds have CODs of 2–5. The majority of optically very thin clouds from the WRF model correspond to high-level cirrus clouds. This is consistent with the result of Cintineo et al. (2013), showing that the Morrison microphysics scheme produces too many upper-level clouds by comparing GOES infrared brightness temperature with the WRF model. Note that the optically-thin multi-layered clouds very likely contain cirrus clouds because their top height is greater than 6 km. The WRF model produces fewer clouds with COD > 1 than observed, and the discrepancy is most apparent for optically very-thick clouds (COD > 50). As a result, the model COD mean and standard deviation are

smaller than those for the retrievals, which are 8.3 and 12.7, respectively for the WRF model, and 17.8 and 30.8, respectively for the GOES retrievals.

4. Impact of cloud errors on photolysis rates

Figure 3 compares the cloudy-sky averaged vertical profiles of NO_2 photolysis rates (JNO_2) predicted by WRF-Chem and measured during the NOMADSS (Fig. 3a) and SEAC^{4}RS (Fig. 3d) campaigns. The histograms of ratio of JNO_2 simulated to that observed under cloudy conditions are also shown for the CNTR and GOES simulations.

For both campaigns, the simulations with satellite clouds (GOES simulations) generally show better agreement with the observed JNO_2 profiles than the ~~control~~CNTR simulations, especially above the boundary layer (above ~2 km). The histograms of the ratio model-to-observation JNO_2 also show a better performance generally in the GOES simulation than in the CNTR simulation: the mean of the ratio is closer to 1 in the GOES simulation than in the CNTR simulation for SEAC^{4}RS, the standard deviations are reduced in the GOES simulation compared to those in the CNTR simulation for both campaigns, the root-mean-square-errors are lowered in the GOES simulation compared to those in the CNTR simulation, and the correlation coefficients are closer to 1 in the GOES simulation than in the CNTR simulation. For NOMADSS, the large bias in the highest ratio bin (> 2) is 24% less in the GOES simulation than in the CNTR simulation. The ~~47%~~ reduction of the large bias ~~(~~>~~(~~bin > 2) in the GOES simulation is more substantial for SEAC^{4}RS~~.~~ ~~This is~~ and reaches 47%. These reductions are attributed to a better representation of the below-cloud and inside-cloud conditions when satellite clouds are used (not shown). ~~The~~This is because the number of data influenced by thick clouds is larger ~~mean model-to-observation JNO_2 ratio and the greater frequency of ratios greater~~in SEAC^{4}RS than ~~1 for~~ in NOMADSS ~~are likely due to~~

~~the overestimation of JNO_2 above clouds as scattered clouds predominate in those~~ and the measurements~~. In the TUV calculations, the clouds in a given grid box (e.g., here a 12 km × 12 km box) are assumed to be infinitely extended in the horizontal direction. However, the sensor can see a broader area (than a 12 km × 12 km area), and so~~ in the presence of ~~scattered~~those thick clouds ~~a~~ were mostly made under below-cloud ~~fraction within sensor view angles can be smaller than 1. Therefore, the modeled JNO_2 can be larger in the presence of scattered clouds as compared to the measured JNO_2~~or inside-cloud conditions.

5. Impact of cloud errors on ground level ozone

5.1. An example on 8 July 2013 in Midwestern US

Figure 4 shows an example of how model errors in cloud fields impact O_3 predictions. This example includes thunderstorm systems over the Midwestern US. The CNTR simulation misses clouds or underpredicts CODs over metropolitan Chicago and the region south of Lake Michigan. This results in the overprediction of JNO_2 by up to 0.54 min^{-1} (~90%) compared to that computed using GOES clouds. The resulting changes in O_3 concentration are regional and the O_3 overprediction in the plume originating from the Chicago area is up to 62 ppb (~60% of O_3 in the CNTR simulation). As a result of the cloud corrections, O_3 in the GOES simulation agrees better with observations in those regions (compare Fig. 4d with Fig. 4e and Figs. 4g,h,i). The time series of O_3 at the three sites (marked in Fig. 4f) near Lake Michigan show particularly improved agreement with observations when satellite clouds are used. The large O_3 biases of 20.5 ppb at 11 ~~LST~~CST at Chicago, IL, 19.2 ppb at 13 ~~LST~~CST at La Porte, IN, and 23.5 ppb at 16 ~~LST~~CST at Holland, MI in the CNTR simulation are reduced to 1.7 ppb, 3.2 ppb, and −0.11 ppb in the GOES simulation, respectively. It is also apparent that the bias reduction in O_3 shifts eastward

(from Chicago, IL to Holland, MI) as the thunderstorm moves eastward during the day. An important implication of this finding is that errors in cloud predictions can lead to wrong O_3 alerts in areas where model does not predict clouds well. For example, the ~~daily~~ maximum ~~daily~~ 8-h ~~O_3~~average O_3 (MDA8 O_3) concentration is 75.3 ppb at Holland, MI in the CNTR simulation (Fig. 4i) and this value exceeds the O_3 standard (70 ppb for ~~8-h~~MDA8 O_3). However, the ~~daily maximum 8-h~~MDA8 O_3 concentration at the same location is 63.0 ppb in the GOES simulation and 60.4 ppb in the observation. Therefore, an O_3 action alert would have been issued if the CNTR simulation results are used, which results in a false alarm. The example shown here emphasizes the important roles of clouds in the Great Lakes region where large O_3 biases have been reported previously in air quality forecasts (e.g., Cleary et al., 2015). The correction of clouds both over the lakes and in the upstream regions (mostly large cities located to the west/southwest of the lakes) significantly reduces the O_3 bias. It is also shown that polluted air masses from the source regions can be advected over the lakes (not shown). In this case in which precursor levels can be high over the lakes, the presence of clouds over the lakes can greatly affect O_3 formation over the lakes.

In general, the regions exhibiting O_3 differences between the two simulations coincide with the regions where JNO_2 values are different. More importantly, large O_3 differences are found near urban areas (e.g., Chicago, IL; downwind area of Kansas City, MO; Omaha, NE and its downwind area). Even though the difference in COD or JNO_2 is significant in central Indiana, for example, the difference in O_3 in the region is relatively small compared to that near Lake Michigan.

5.2. Maximum daily 8-h average O_3

Figure 5 shows the maps of MDA8 O_3 averaged over the study period for the CNTR simulation and the difference in MDA8 O_3 between the CNTR and GOES simulations. The spatial distribution of ~~8-h average O_3 (10–17 LST average, simply 8-h O_3 hereafter) averaged over the whole study period~~ MDA8 O_3 in the GOES simulation is similar to that in the CNTR simulation~~,~~ (thus the GOES spatial average is not shown here), but the O_3 levels are considerably different. ~~Figure 5 shows the maps of 8-h O_3 for the CNTR simulation and the O_3 difference between the CNTR and GOES simulations.~~ In Fig. 5b, the Midwestern, eastern, and northwestern US regions show the largest O_3 differences, up to ~~4.7~~5.8 ppb, with lower O_3 levels in the GOES simulation. These regions generally belong to the contingency category C (Midwestern and northwestern US) or category A (eastern US). On the other hand, the regions with negative differences, i.e., some places over the south/southeastern US, coincide with the contingency category B. These differences are expected and can be interpreted as follows: when the WRF model misses clouds (clear sky in the CNTR simulation, category C) or underestimates COD (as seen in Fig. 2), surface O_3 is overestimated. When the WRF model generates clouds that are not present in reality (clear sky in the satellite retrievals, category B), surface O_3 is underestimated. It should be noted that not all regions belonging to category B or C have significant O_3 differences. Interestingly, the regions exhibiting significantly large O_3 differences coincide with large urban areas, e.g., Seattle, WA; Los Angeles, CA; Chicago, IL; Cleveland, OH; Houston, TX; New Orleans, LA; Atlanta, GA; and Miami, FL. The reasons for this result are explored in section 5.4 and 5.5.

The performance of the GOES simulation is found to be better than that of the CNTR simulation as compared to observations: for example, under cloudy conditions (COD > 20, see section 5.4

for the criterion), the root-mean-square error of MDA8 O_3 in the GOES (CNTR) simulation is 13.2 ppb (16.9 ppb) and the correlation coefficient of MDA8 O_3 in the GOES (CNTR) simulation is 0.5 (0.4).

5.3. Relative contribution to O_3 errors from photolysis rates and BVOC emissions

It is expected that reduced BVOC emissions (especially isoprene) due to the presence of clouds can also decrease O_3 formation. Figure 6 shows the spatial distributions of relative changes in PAR and isoprene emission between the EMIS_BVOC and GOES simulations averaged over a 10-day period. Because the WRF model tends to underestimate COD or is not able to reproduce clouds in Midwestern and western US, PAR and biogenic isoprene emissions are larger in the EMIS_BVOC simulation than in the GOES simulation. On the other hand, the model overestimates COD or produces clouds that are not present in reality over the southeast US, so PAR and biogenic isoprene emissions are lower in the EMIS_BVOC simulation than in the GOES simulation. The change in PAR (biogenic isoprene emissions) resulting from the difference in clouds fields between the WRF model and satellite retrievals is up to ±30–40% (±25%). ~~The~~Figure 6d shows the relative O_3 difference between ~~the~~ EMIS_BVOC and GOES simulations ~~(Fig. 6d) is relatively small in comparison~~ to ~~the~~ O_3 difference ~~in O_3~~ between ~~the~~ CNTR and GOES simulations (Fig. 6c~~)~~). It is seen that ~~results from both photolysis rate and BVOC emission changes. In general,~~ the contribution of changes in BVOC emissions is considerable only for some regions and it ranges from ~10–40%. The average contribution of changes in BVOC emissions over land is ~20% compared to changes of BVOC emissions plus photolysis rates ~~to changes in O_3 is ~80%, on average, over CONUS and the remaining (~20%) is attributed to changes in BVOC emissions.~~using GOES satellite clouds. The contribution of BVOC emissions is larger ~~(up to ~~(~40%) in urban areas over the southeast (specifically in

Charlotte, NC). The difference in O_3 in Charlotte, NC resulting from changes in BVOC emissions is about 1.5 ppb and that from changes in both photolysis rates and BVOC emissions is about 3.5 ppb. In some regions, such as Midwestern, western Pennsylvania, and central New York, the effect of BVOC emissions is negligible.

5.4. Cloud effects on ozone bias in VOC- and NO_X -limited regimes

In this section, we examine the effects of clouds on O_3 in VOC-limited and NO_X-limited regimes in order to understand the reasons for a stronger O_3 response to cloud corrections in urban areas than in the remote regions. Figure 7 shows how cloud corrections affect O_3 errors in different regimes. Here, ~~8-h~~MDA8 O_3 is used to compute the model O_3 bias (simulation minus observation). Figures 7a and 7b show the probability density functions of the model O_3 bias for the CNTR and GOES simulations, respectively, at all ground sites experiencing considerably thick (COD > 20) clouds. In this example, an EPA site is considered under cloudy sky conditions when hourly COD greater than the chosen threshold (here, 20) is present at the site for at least 4 hours within the 8-h time window in a given day. The decrease in the O_3 bias for VOC-limited regime is significant, and the difference in median values between the two simulations is 5.~~4~~2 ppb. The decrease in O_3 bias for NO_X-limited regimes (2.~~75~~7 ppb) is about 2 times smaller than that for VOC-limited regime. An important result is that the frequency of very large biases (e.g., greater than 20 ppb) is substantially reduced when cloud fields are corrected, especially for the VOC-limited regime. This implies that more accurate cloud predictions ultimately improve the accuracy of O_3 alert predictions, especially in polluted urban areas.

Figure 7c shows the change in median values of ~~8 h~~MDA8 O_3 bias for a range of COD thresholds. We find that the O_3 bias increases with increasing cloudiness in the CNTR simulation. As previously mentioned, the O_3 bias is generally larger for VOC-limited regimes than for NO_X-limited regimes. When the radiation fields are corrected with satellite clouds, the model O_3 bias is considerably reduced (but not zero). In addition, the O_3 bias in the GOES simulation does not increase as much as that in the CNTR simulation when cloudiness increases. This implies that there are other sources of O_3 biases in the GOES simulation, which are not likely associated with cloudiness. The other errors sources can be precursor emissions, mixing/transport, and deposition. Fig. 7d compares the median values of ~~8 h~~MDA8 O_3 bias between the two simulations (CNTR minus GOES), and shows that the difference in ~~8 h~~MDA8 O_3 between the two simulations clearly increases as the COD threshold increases and that the effect of cloud correction is larger in VOC-limited than in NO_X-limited regimes. The reduced O_3 bias as a result of cloud corrections ranges from 1 to ~~6~~5 ppb depending on CODs and chemistry regimes. This represents up to ~40% of the total O_3 bias under cloudy conditions in the current model version (e.g., 5.~~4~~2 ppb of ~~13.37~~12.6 ppb for COD threshold of 20 in VOC-limited regimes). Note that the results for the sites in transitional zone (the slope of $\Delta O_3/\Delta NO_y$ is 4–6) showed that the effects of cloud in the transitional zone are intermediate; that is, larger than those for NO_X-limited regimes but smaller than those for VOC-limited regimes (not shown).

We performed additional analysis by dividing VOC- and NO_X-limited sites into groups that have similar ranges of peak MDA8 O_3 concentration during the period of June–September 2013 (Fig. S3). All sites are grouped into bins with peak value of MDA8 O_3 ranging from larger than 75 ppb, 70–75 ppb, 65–70 ppb, 60–65 ppb, to smaller than 60 ppb. The maximum reduction in O_3 bias due to cloud corrections is obtained for the VOC-limited sites with peak MDA8 O_3 of 65–70

ppb and reaches ~8 ppb. The maximum reduction for NO_X-limited sites, on the other hand, is ~4 ppb and found for the sites with peak MDA8 O_3 of 70–75 ppb. Although the degree of the O_3 bias reduction varies somewhat among the bins for a given ozone regime, the effects of cloud correction on O_3 bias reduction remain larger in VOC-limited regimes than NO_X-limited regimes.

We examine the O_3 bias over the southeast US where large overpredictions at the surface have been reported (e.g., Travis et al. 2016) in ~~a~~ the supplementary ~~section.~~material. It is found that a considerable portion of O_3 bias is attributable to inaccurate cloud predictions over the southeast US, but the degree of the effects of clouds is smaller than that over CONUS as a whole (Fig. ~~S2~~S4). The maximum reduction in O_3 bias due to inaccurate cloud predictions is 4.~~6~~5 ppb over the southeast US and 5.~~7~~3 ppb over CONUS. Still, large O_3 biases of ~11 ppb are present over the southeast US (compared to those of ~~8~~6–9 ppb over CONUS) even though the ~~cloud~~ clouds and radiation fields that are ~~corrected for~~ relevant to photochemistry~~. are corrected.~~ This result implies that errors resulting from other processes exist and are responsible for the surface O_3 overpredictions over the southeast US. More in-depth studies that find and quantify errors are therefore required to better predict the O_3 over the southeast US as well as CONUS.

5.5. Ozone formation sensitivity to changes in photolysis rates

The difference in O_3 sensitivity to changes in photolysis rates (resulting from the presence of clouds) in different regimes is determined by calculating $d\ln(O_3)/d\ln(JNO_2)$ ratios as in Kleinman (1991). Table 3 lists those sensitivity coefficients of O_3 to JNO_2 and shows that O_3 is more sensitive to JNO_2 in VOC-limited than in NO_X-limited regimes, being 1.69 times larger under cloudy-sky conditions and by 1.65 times greater under clear-sky conditions. Similar

sensitivities were reported for OH by Berresheim et al. (2003) with the sensitivity of OH to JO^1D, $d\ln(OH)/d\ln(JO^1D)$, of 0.8 at high NO_2 levels (~10 ppb) and 0.68 at low to moderate NO_2 levels (~1 ppb). The corresponding sensitivities from our study are 1.1 for VOC-limited regimes and 0.66 for NO_X-limited regimes under clear-sky conditions. Similar results are also found for the net chemical production of O_3 and OH concentration, revealing stronger responses to changes in cloudiness in VOC-limited regimes than NO_X-limited regimes (Fig. 8). It is interesting to note that OH and HO_2 have local maxima at CODs between 2 and 5. As shown in Ryu et al. (2017), the enhancement of actinic flux at the surface due to optically thin clouds (CODs < 5) is considerable for high-level clouds, i.e., cirrus. The local maxima, therefore, likely result from the fact that the GOES clouds have the largest portion of cirrus for CODs of 2–5 as seen in Fig. 2b. Figure 8 also shows that the variation (defined by 25 and 75 percentiles) of net chemical production of O_3 with respect to COD is much larger in VOC-limited conditions. This result suggests that predicting O_3 under cloudy conditions is likely more difficult in VOC-limited than in NO_X-limited regimes. It is also noticeable that the HO_2 radical concentration remains relatively high in NO_X-limited regimes even under cloudy conditions as compared to the VOC-limited regimes. Note that the results of WRF-Chem here include the effects of both photolysis rates and BVOC emissions.

A simplified box model (BOXMOX, Knote et al. (2015)) simulation using the same chemical mechanism (MOZART-4) as WRF-Chem was performed to better understand O_3 sensitivity to changing cloudiness in different chemistry regimes. The emission rates for VOC-limited (NO_X-limited) regime are those of the Chicago urban (rural) area in the WRF-Chem simulation. The initial conditions are taken from the CNTR simulation at 09 ~~LST~~CST 7 July 2013 in the Chicago suburban area for both regimes. Dry deposition is not considered. Photolysis rates for all species

that are photodissociable are varied from clear-sky to cloudy conditions with up to 80% reduction. The 80% reduction roughly corresponds to COD of 35 (not shown). The box model is integrated for ~~12~~3 hours and photolysis rates are kept constant during the simulation (i.e., no diurnal variations). The box model results are found to be consistent with the results from the WRF-Chem simulations: the variations of O_3 and OH with respect to decreasing photolysis rates are larger in VOC-limited regime than in NO_X-limited regime (Fig. ~~S3~~S5, in the supplementary~~).~~ material). Note that the net chemical production of O_3 obtained from the box model results also shows a larger sensitivity to cloudiness in VOC-limited regimes than in NO_X-limited regimes, which is similar to Figs. 8a and 8d (not shown). Figure 9 shows production and loss terms of RO_X (= OH + HO_2 + RO_2) radicals with variations in photolysis rates for VOC-limited and NO_X-limited regimes. In both regimes, the decreased sunlight due to clouds reduces OH formation by photodissociation of O_3 (primary source of OH). The larger sensitivity of OH radicals to COD in VOC-limited regimes as seen in Fig. 8 is associated with the loss of OH by the radical termination reaction between OH and NO_2 under NO_X-rich conditions, which leads to the large decrease in OH (Fig. 9a). On the other hand, in NO_X-limited regimes, the radical termination reactions are the radical-radical reactions (Fig. 9b). In this regime, OH mainly reacts with VOCs and propagates through radical cycles by producing HO_2/RO_2 radicals, rather than being terminated by the reaction with NO_2. Given that the reaction between NO and HO_2 becomes the largest source of OH budget (secondary source of OH) at an NO_X concentration of ~1 ppb (Ehhalt and Rohrer, 2000; Eisele et al., 1997), OH can be relatively less sensitive to the changes in radiation. Note that the mean daytime NO_X concentration over CONUS in NO_X-limited regimes is 1.2 ppb and that in VOC-limited regimes is 6.7 ppb for this study period. Another attribute is a ~~relatively~~ greater contribution of H_2O_2 photodissociation to the production of RO_X

in NO_X-limited regimes than that of HNO_3, which is negligible. Unlike the radical terminated in VOC-limited conditions, a non-negligible amount of terminated radicals can be recycled in the NO_X-limited regime.

6. Sensitivity of cloud optical depth and O_3 to microphysics ~~scheme~~and convective schemes

It should be emphasized that our study was performed using a specific representation of the cloud microphysics by Morrison et al. ~~(2009).~~(2009) and cumulus parameterization (Grell and Devenyi, 2002). To test the robustness of our results with regard to the representation of clouds, another microphysics scheme, Thompson scheme (Thompson et al., 2008), is employed for a 10-day (3 July–12 July 2013) sensitivity simulation. The COD comparison in Fig. ~~S4~~S6 shows that with the Thompson scheme the model predicts fewer clouds for all ranges of CODs as compared to GOES retrievals, except for the very thin ones (COD < 1) in which the number of those clouds is still overpredicted as seen in the simulation with Morrison scheme. Compared to the Morrison scheme, the Thompson scheme produces significantly less high-level (cirrus) clouds. This is also consistent with the findings of Cintineo et al. (2013). Despite this difference, the shape of the COD distribution from the two microphysics schemes are rather similar to each other.

The ~~8-h~~MDA8 O_3 bias with the Thompson scheme is evaluated (Fig. ~~S5~~S7), and compared to that of the Morrison scheme for the same period. ~~The~~Under the conditions of COD greater than 20, for example, the baseline simulation with the Thompson scheme (that uses model generated clouds) shows that a median bias (14.~~09~~79 ppb) is a bit smaller than that with the Morrison scheme (16.~~29~~22 ppb) for that period in VOC-limited regimes. In the sensitivity simulation with

the Thompson scheme that uses GOES satellite clouds for photochemistry, the median bias is reduced by ~~6.07~~5.45 ppb (~~43~~37%, Fig. ~~S5a~~S7a) in VOC-limited regimes and by ~~1.45~~2.06 ppb (~~14~~20%, Fig. ~~S5c~~S7c) in NO_X-limited regimes, which are consistent with the results of our base simulation. The degree of the effects of cloud correction in the sensitivity simulations with the Thompson scheme, ranging from 0.5 to ~~6~~5.5 ppb, is similar to that found in ~~the simulations~~our base simulation with the Morrison scheme. Therefore, the general conclusions remain the same: i.e~~.~~., errors in O_3 predictions resulting from errors in cloud predictions are considerable (up to ~~6~~5 ppb on average) and the effects of cloud corrections are larger in VOC-limited regimes than in NO_X-limited regimes.

To estimate the sensitivity of our results to cumulus parameterization schemes, sensitivity simulations with the Grell-Freitas scheme (Grell and Freitas, 2014) are performed. As done for microphysics scheme, a period of 10 days (3–12 July 2013) was considered. In Fig. S8, the histograms of cloud optical depths obtained for the 10-day period from Grell-Freitas scheme and from Grell-3D scheme show that the distributions of cloud optical depths are in general similar to each other. The Grell-Freitas scheme tends to produce fewer clouds with small or moderate cloud optical depths (Fig. S8). As shown in Fig. S9, the degree of cloud correction in reducing O_3 bias is larger in VOC-limited regimes than in NO_X-limited regimes in the simulation with Grell-Freitas scheme, and thus the conclusions originally drawn remain unchanged.

7. Conclusions and discussion

We performed quantitative analyses ~~with~~of the WRF-Chem model meso-scale (12 km) simulations to determine how much errors in cloud predictions contribute to errors in surface O_3

predictions during summertime over CONUS. Clouds were generated using the Morrison microphysics and Grell 3D cumulus parameterization schemes. It is found that the WRF-Chem model is able to generate roughly 55% of the clouds in the right locations by comparing to satellite clouds. A quantitative comparison of COD shows that the WRF-Chem model predicts too many thin cirrus clouds with CODs less than 1, and also considerably underpredicts the optical depths for a majority of cloud systems.

The errors in cloud predictions can lead to large hourly O_3 biases of up to 60 ppb, for example, for specific cases in which the model misses deep convective clouds that are present in reality. On average, the errors in ~~8-h~~MDA8 O_3 of 1–~~6~~5 ppb are found to be attributable to errors in cloud predictions under cloudy sky conditions. We quantify separately the contribution of changes in photolysis rates and emissions of light-dependent BVOCs to cloud-related errors in surface O_3. The contribution of photolysis rates to surface O_3 is larger (~80% on average) than that of BVOC emissions. The contribution of BVOC emissions to O_3 can become important (~40%) in the VOC-limited regimes where BVOC emissions are large (i.e., cities of the southeast US).

The effects of cloud corrections are more impactful in VOC-limited (or high-NO_X) than in NO_X-limited (or low-NO_X) regimes. The sensitivity of O_3 with respect to COD is about 2 times larger in VOC-limited than in NO_X-limited regimes. This finding is consistent with the box modeling results that were performed for typical urban ~~(~~/rural~~)~~ conditions under varying photolysis rates. The production of radicals (OH, HO_2, and RO_2) decreases with decreasing photolysis rates in the presence of clouds. The primary reason for the larger sensitivity of O_3 formation to clouds in VOC-limited regimes is that the loss of OH is much stronger in VOC-limited regimes due to the reaction with NO_2. Thus, OH cannot readily propagate through the radical cycles. In NO_X-limited regimes, the radicals terminated from the radical cycles are mostly HO_2 and RO_2 rather

than OH. Thus, OH can remain in the cycles and continue to produce HO_2 and RO_2 by reacting with VOCs before termination. The interconversion of HO_2 to OH is the dominant process in NO_X-limited regimes, and therefore OH and O_3 formations are less sensitive to changes in radiation.

~~This study suggests that accurate cloud predictions through data assimilation or cloud mask corrections with near-real time satellite cloud data would benefit accurate O_3 predictions and that the benefit is expected to be greater in VOC-limited than in NO_X-limited regimes. Even though~~We showed that considerable reduction in O_3 bias is achieved by correcting cloud-related radiation fields; however, O_3 is still overpredicted by the WRF-Chem model. The remaining bias likely results from other processes involved in the O_3 lifecycle such as precursor emissions from both anthropogenic and biogenic sources, transport, turbulent mixing, and dry deposition, which quantitative assessment is beyond the scope of this study.

One should keep in mind that the quantitative estimate of the O_3 bias related to the cloud effects on radiation as reported in this study could be sensitive to several factors. In particular, this study is based on a particular configuration of the WRF-Chem model with regard to the radiation, microphysics, cumulus, boundary layer parameterization and the chemistry scheme. We have tested the sensitivity of our results to the choice of microphysics and cumulus parameterization schemes, and have shown that ~~the 8-h~~MDA8 O_3 biases are reduced by up to ~~6~~5 ppb with the satellite cloud corrections in the simulations with the ~~Thompson microphysis scheme~~different microphysics and cumulus parameterization schemes, which is consistent with the results found in our base simulations ~~with the Morrison microphysis scheme.~~.

~~From the perspective of O_3 forecast, it is expected that errors in O_3 predictions are greater when the initial and boundary conditions for WRF-Chem simulations are provided by meteorological forecasts compared to those simulations in which the initial and boundary conditions are provided by meteorological reanalysis because the reanalysis data are an improved estimate of the meteorological state. Understanding the evolution of errors in O_3 forecast associated with errors in cloud forecast and optimizing the use of meteorological forecasts for better O_3 forecast skill are therefore necessary and will be addressed in a future study.~~This study suggests that accurate cloud predictions through data assimilation or cloud mask corrections with near-real time satellite cloud data would improve the accuracy of O_3 predictions and that the benefit is expected to be greater in VOC-limited than in NO_X-limited regimes. It should be noted that our estimates are based on WRF-Chem simulations that use initial and boundary conditions from meteorological analysis data, which is an improved estimate of the meteorological state compared to forecast data, and thus the reduction of errors in O_3 predictions could be even greater in a forecasting setting. From the perspective of O_3 forecast, our study indicates that there is a need for an enhanced understanding of the evolution of errors in O_3 forecasts associated with errors in cloud forecasts, and for optimizing the use of meteorological forecasts to allow more accurate near-term O_3 predictions. The present study corrects cloud fields in WRF using satellite clouds only for radiation that is relevant to photochemistry, and those cloud corrections do not affect other meteorological variables such as surface temperature, wind, humidity, boundary layer height, etc. In a future study, we plan to examine the effects of satellite cloud assimilation on near-term O_3 forecasts using enhanced forecasts such as the Rapid Refresh products from NOAA (Benjamin et al., 2016) that take into account cloud data assimilation to derive meteorology. The Rapid Refresh uses satellite cloud products as well as cloud observations from

the ground and considers the thermodynamic balance between temperature and humidity due to the presence of clouds. Thus, this will allow investigating the effects of cloud assimilation on O_3 forecasts not only through changes in radiation for photochemistry but also through changes in meteorological variables.

Acknowledgments

We acknowledge Samuel Hall and Kirk Ullmann for providing actinic flux data that are used for supplementary analysis, George Grell and Geoff Tyndall ~~and George Grell~~ for helpful discussions. This study is supported from NASA-ROSES grant NNX15AE38G. P. Minnis was supported by the NASA Modeling, Analysis, and Prediction Program. The National Center for Atmospheric Research is sponsored by the National Science Foundation. We would like to acknowledge high-performance computing support from Cheyenne (doi:10.5065/D6RX99HX) provided by NCAR's Computational and Information Systems Laboratory, sponsored by the National Science Foundation. The GOES cloud retrievals are available at https://satcorps.larc.nasa.gov. The EPA ozone data can be downloaded at https://aqsdr1.epa.gov/aqsweb/aqstmp/airdata/download_files.html.

620

621

622

623

624

625

626

627 **Reference**

628 Bei, N., Lei, W., Zavala, M. and Molina, L. T.: Ozone predictabilities due to meteorological
629 uncertainties in the Mexico City basin using ensemble forecasts, Atmos Chem Phys, 10(13),
630 6295–6309, doi:10.5194/acp-10-6295-2010, 2010.

631 Benjamin, S. G., Weygandt, S. S., Brown, J. M., Hu, M., Alexander, C. R., Smirnova, T. G.,
632 Olson, J. B., James, E. P., Dowell, D. C., Grell, G. A., Lin, H., Peckham, S. E., Smith, T. L.,
633 Moninger, W. R., Kenyon, J. S. and Manikin, G. S.: A North American Hourly Assimilation and
634 Model Forecast Cycle: The Rapid Refresh, Mon. Wea. Rev., 144(4), 1669–1694,
635 doi:10.1175/MWR-D-15-0242.1, 2015.

636 Berresheim, H., Plass-Dülmer, C., Elste, T., Mihalopoulos, N. and Rohrer, F.: OH in the coastal
637 boundary layer of Crete during MINOS: Measurements and relationship with ozone photolysis,
638 Atmos Chem Phys, 3(3), 639–649, doi:10.5194/acp-3-639-2003, 2003.

639 Briegleb, B. P.: Delta-Eddington approximation for solar radiation in the NCAR community
640 climate model, J. Geophys. Res. Atmospheres, 97(D7), 7603–7612, doi:10.1029/92JD00291,
641 1992.

642 Brioude, J., Angevine, W. M., Ahmadov, R., Kim, S.-W., Evan, S., McKeen, S. A., Hsie, E.-Y.,
643 Frost, G. J., Neuman, J. A., Pollack, I. B., Peischl, J., Ryerson, T. B., Holloway, J., Brown, S. S.,
644 Nowak, J. B., Roberts, J. M., Wofsy, S. C., Santoni, G. W., Oda, T. and Trainer, M.: Top-down
645 estimate of surface flux in the Los Angeles Basin using a mesoscale inverse modeling technique:
646 assessing anthropogenic emissions of CO, NOx and CO2 and their impacts, Atmos Chem Phys,
647 13(7), 3661–3677, doi:10.5194/acp-13-3661-2013, 2013.

Brown-Steiner, B., Hess, P. G. and Lin, M. Y.: On the capabilities and limitations of GCCM simulations of summertime regional air quality: A diagnostic analysis of ozone and temperature simulations in the US using CESM CAM-Chem, Atmos. Environ., 101, 134–148, doi:10.1016/j.atmosenv.2014.11.001, 2015.

Campbell, P., Zhang, Y., Yahya, K., Wang, K., Hogrefe, C., Pouliot, G., Knote, C., Hodzic, A., San Jose, R., Perez, J. L., Jimenez Guerrero, P., Baro, R. and Makar, P.: A multi-model assessment for the 2006 and 2010 simulations under the Air Quality Model Evaluation International Initiative (AQMEII) phase 2 over North America: Part I. Indicators of the sensitivity of O3 and PM2.5 formation regimes, Atmos. Environ., 115, 569–586, doi:10.1016/j.atmosenv.2014.12.026, 2015.

Carter, W. P. L.: Development of the SAPRC-07 chemical mechanism, Atmos. Environ., 44(40), 5324–5335, doi:10.1016/j.atmosenv.2010.01.026, 2010.

Chang, J. S., Brost, R. A., Isaksen, I. S. A., Madronich, S., Middleton, P., Stockwell, W. R. and Walcek, C. J.: A three-dimensional Eulerian acid deposition model: Physical concepts and formulation, J. Geophys. Res. Atmospheres, 92(D12), 14681–14700, doi:10.1029/JD092iD12p14681, 1987.

Chen, F. and Dudhia, J.: Coupling an Advanced Land Surface–Hydrology Model with the Penn State–NCAR MM5 Modeling System. Part I: Model Implementation and Sensitivity, Mon. Weather Rev., 129(4), 569–585, doi:10.1175/1520-0493(2001)129<0569:CAALSH>2.0.CO;2, 2001.

668 Cintineo, R., Otkin, J. A., Xue, M. and Kong, F.: Evaluating the Performance of Planetary
669 Boundary Layer and Cloud Microphysical Parameterization Schemes in Convection-Permitting
670 Ensemble Forecasts Using Synthetic GOES-13 Satellite Observations, Mon. Weather Rev.,
671 142(1), 163–182, doi:10.1175/MWR-D-13-00143.1, 2013.

672 Cleary, P. A., Fuhrman, N., Schulz, L., Schafer, J., Fillingham, J., Bootsma, H., McQueen, J.,
673 Tang, Y., Langel, T., McKeen, S., Williams, E. J., and Brown, S. S.: Ozone distributions over
674 southern Lake Michigan: comparisons between ferry-based observations, shoreline-based DOAS
675 observations and model forecasts, Atmos. Chem. Phys., 15, 5109-5122,
676 https://doi.org/10.5194/acp-15-5109-2015, 2015.

677 Dabberdt, W. F., Carroll, M. A., Baumgardner, D., Carmichael, G., Cohen, R., Dye, T., Ellis, J.,
678 Grell, G., Grimmond, S., Hanna, S., Irwin, J., Lamb, B., Madronich, S., McQueen, J., Meagher,
679 J., Odman, T., Pleim, J., Schmid, H. P. and Westphal, D. L.: Meteorological Research Needs for
680 Improved Air Quality Forecasting: Report of the 11th Prospectus Development Team of the U.S.
681 Weather Research Program*, Bull. Am. Meteorol. Soc., 85(4), 563–586, doi:10.1175/BAMS-85-
682 4-563, 2004.

683 Ehhalt, D. H. and Rohrer, F.: Dependence of the OH concentration on solar UV, J. Geophys. Res.
684 Atmospheres, 105(D3), 3565–3571, doi:10.1029/1999JD901070, 2000.

685 Eisele, F. L., Mount, G. H., Tanner, D., Jefferson, A., Shetter, R., Harder, J. W. and Williams, E.
686 J.: Understanding the production and interconversion of the hydroxyl radical during the
687 Tropospheric OH Photochemistry Experiment, J. Geophys. Res. Atmospheres, 102(D5), 6457–
688 6465, doi:10.1029/96JD02207, 1997.

689 Fiore, A. M., Dentener, F. J., Wild, O., Cuvelier, C., Schultz, M. G., Hess, P., Textor, C., Schulz,
690 M., Doherty, R. M., Horowitz, L. W., MacKenzie, I. A., Sanderson, M. G., Shindell, D. T.,
691 Stevenson, D. S., Szopa, S., Van Dingenen, R., Zeng, G., Atherton, C., Bergmann, D., Bey, I.,
692 Carmichael, G., Collins, W. J., Duncan, B. N., Faluvegi, G., Folberth, G., Gauss, M., Gong, S.,
693 Hauglustaine, D., Holloway, T., Isaksen, I. S. A., Jacob, D. J., Jonson, J. E., Kaminski, J. W.,
694 Keating, T. J., Lupu, A., Marmer, E., Montanaro, V., Park, R. J., Pitari, G., Pringle, K. J., Pyle, J.
695 A., Schroeder, S., Vivanco, M. G., Wind, P., Wojcik, G., Wu, S. and Zuber, A.: Multimodel
696 estimates of intercontinental source-receptor relationships for ozone pollution, J. Geophys. Res.
697 Atmospheres, 114(D4), D04301, doi:10.1029/2008JD010816, 2009.

698 Grell, G. A. and Devenyi, D.: A generalized approach to parameterizing convection combining
699 ensemble and data assimilation techniques, Geophys. Res. Lett., 29(14), 38–1,
700 doi:10.1029/2002GL015311, 2002.

701 Grell, G. A. and Freitas, S. R.: A scale and aerosol aware stochastic convective parameterization
702 for weather and air quality modeling, Atmos. Chem. Phys., 14, 5233–5250,
703 https://doi.org/10.5194/acp-14-5233-2014, 2014.

704 Guenther, A., Karl, T., Harley, P., Wiedinmyer, C., Palmer, P. I. and Geron, C.: Estimates of
705 global terrestrial isoprene emissions using MEGAN (Model of Emissions of Gases and Aerosols
706 from Nature), Atmos Chem Phys, 6(11), 3181–3210, doi:10.5194/acp-6-3181-2006, 2006.

707 Hodzic, A., Ryu, Y.-H., Madronich, S., Walters, S.: Modeling and evaluation of actinic fluxes
708 and photolysis rates in WRF-Chem, In preparation.

709 Iacono, M. J., Delamere, J. S., Mlawer, E. J., Shephard, M. W., Clough, S. A. and Collins, W. D.:
710 Radiative forcing by long-lived greenhouse gases: Calculations with the AER radiative transfer
711 models, J. Geophys. Res. Atmospheres, 113(D13), D13103, doi:10.1029/2008JD009944, 2008.

712 Im, U., Bianconi, R., Solazzo, E., Kioutsioukis, I., Badia, A., Balzarini, A., Baró, R., Bellasio, R.,
713 Brunner, D., Chemel, C., Curci, G., Flemming, J., Forkel, R., Giordano, L., Jiménez-Guerrero, P.,
714 Hirtl, M., Hodzic, A., Honzak, L., Jorba, O., Knote, C., Kuenen, J. J. P., Makar, P. A., Manders-
715 Groot, A., Neal, L., Pérez, J. L., Pirovano, G., Pouliot, G., San Jose, R., Savage, N., Schroder,
716 W., Sokhi, R. S., Syrakov, D., Torian, A., Tuccella, P., Werhahn, J., Wolke, R., Yahya, K.,
717 Zabkar, R., Zhang, Y., Zhang, J., Hogrefe, C. and Galmarini, S.: Evaluation of operational on-
718 line-coupled regional air quality models over Europe and North America in the context of
719 AQMEII phase 2. Part I: Ozone, Atmos. Environ., 115, 404–420,
720 doi:10.1016/j.atmosenv.2014.09.042, 2015.

721 Kleinman, L. I.: Seasonal dependence of boundary layer peroxide concentration: The low and
722 high NO x regimes, J. Geophys. Res. Atmospheres, 96(D11), 20721–20733,
723 doi:10.1029/91JD02040, 1991.

724 Knote, C., Hodzic, A., Jimenez, J. L., Volkamer, R., Orlando, J. J., Baidar, S., Brioude, J., Fast,
725 J., Gentner, D. R., Goldstein, A. H., Hayes, P. L., Knighton, W. B., Oetjen, H., Setyan, A., Stark,
726 H., Thalman, R., Tyndall, G., Washenfelder, R., Waxman, E. and Zhang, Q.: Simulation of semi-
727 explicit mechanisms of SOA formation from glyoxal in aerosol in a 3-D model, Atmos Chem
728 Phys, 14(12), 6213–6239, doi:10.5194/acp-14-6213-2014, 2014.

729 Knote, C., Tuccella, P., Curci, G., Emmons, L., Orlando, J. J., Madronich, S., Baró, R., Jiménez-
730 Guerrero, P., Luecken, D., Hogrefe, C., Forkel, R., Werhahn, J., Hirtl, M., Pérez, J. L., San José,

731 R., Giordano, L., Brunner, D., Yahya, K. and Zhang, Y.: Influence of the choice of gas-phase
732 mechanism on predictions of key gaseous pollutants during the AQMEII phase-2
733 intercomparison, Atmos. Environ., 115, 553–568, doi:10.1016/j.atmosenv.2014.11.066, 2015.

734 Lin, M., Horowitz, L. W., Payton, R., Fiore, A. M. and Tonnesen, G.: US surface ozone trends
735 and extremes from 1980 to 2014: quantifying the roles of rising Asian emissions, domestic
736 controls, wildfires, and climate, Atmos Chem Phys, 17(4), 2943–2970, doi:10.5194/acp-17-
737 2943-2017, 2017.

738 Mayer, B., Fischer, C. A. and Madronich, S.: Estimation of surface actinic flux from satellite
739 (TOMS) ozone and cloud reflectivity measurements, Geophys. Res. Lett., 25(23), 4321–4324,
740 doi:10.1029/1998GL900140, 1998.

741 Minnis, P., Nguyen, L., Palikonda, R., Heck, P. W. Spangenberg, D. A., Doelling, D. R., Ayers,
742 J. K., Smith, W. L., Jr., Khaiyer, M. M., Trepte, Q. Z., Avey, L. A., Chang, F.-L., Yost, C. R.,
743 Chee, T. L., and Sun-Mack, S.: Near-real time cloud retrievals from operational and research
744 meteorological satellites, Proc. SPIE Remote Sens. Clouds Atmos. XIII, 7107-2, 8 pp., ISBN:
745 9780819473387, 2008.

746 Minnis, P., Sun-Mack, S., Trepte, Q. Z., Chang, F.-L., Heck, P. W., Chen, Y., Yi, Y., Arduini, R.
747 F., Ayers, K., Bedka, K., Bedka, S., Brown, R., Gibson, S., Heckert, E., Hong, G., Jin, Z.
748 Palikonda, R. Smith, R. Smith, W. l., Jr., Spangenberg, D. A. Yang, P., Yost, C. R., and Xie,
749 Y.: CERES Edition 3 cloud retrievals. *AMS 13th Conf. Atmos. Rad.*, Portland, OR, June 27 – July
750 2, 5.4, 7 pp., 2010.

751 Minnis, P., Sun-Mack, S., Young, D. F., Heck, P. W., Garber, D. P., Chen, Y., Spangenberg, D.
752 A., Arduini, R. F., Trepte, Q. Z., Smith, W. L., Ayers, J. K., Gibson, S. C., Miller, W. F., Hong,

753 G., Chakrapani, V., Takano, Y., Liou, K. N., Xie, Y. and Yang, P.: CERES Edition-2 Cloud
754 Property Retrievals Using TRMM VIRS and Terra and Aqua MODIS Data #x2014;Part I:
755 Algorithms, IEEE Trans. Geosci. Remote Sens., 49(11), 4374–4400,
756 doi:10.1109/TGRS.2011.2144601, 2011.

757 Minnis, P., Bedka, K., Q. Trepte, Q., Yost, C. R., Bedka, S. T., Scarino, B., Khlopenkov, K., and
758 Khaiyer, M. M., 2016: A consistent long-term cloud and clear-sky radiation property dataset
759 from the Advanced Very High Resolution Radiometer (AVHRR), Climate Algorithm
760 Theoretical Basis Document (C-ATBD), CDRP-ATBD-0826 Rev 1 AVHRR Cloud Properties -
761 NASA, NOAA CDR Program, 19 September, 159 pp.,DOI:10.789/V5HT2M8T, 2016.

762 Morrison, H., Thompson, G. and Tatarskii, V.: Impact of Cloud Microphysics on the
763 Development of Trailing Stratiform Precipitation in a Simulated Squall Line: Comparison of
764 One- and Two-Moment Schemes, Mon. Weather Rev., 137(3), 991–1007,
765 doi:10.1175/2008MWR2556.1, 2009.

766 Nakanishi, M. and Niino, H.: An Improved Mellor–Yamada Level-3 Model: Its Numerical
767 Stability and Application to a Regional Prediction of Advection Fog, Bound.-Layer Meteorol.,
768 119(2), 397–407, doi:10.1007/s10546-005-9030-8, 2006.

769 Pour-Biazar, A., McNider, R. T., Roselle, S. J., Suggs, R., Jedlovec, G., Byun, D. W., Kim, S.,
770 Lin, C. J., Ho, T. C., Haines, S., Dornblaser, B. and Cameron, R.: Correcting photolysis rates on
771 the basis of satellite observed clouds, J. Geophys. Res. Atmospheres, 112(D10), D10302,
772 doi:10.1029/2006JD007422, 2007.

773 Rossow, W. B. and Schiffer, R. A.: Advances in Understanding Clouds from ISCCP, Bull. Am.
774 Meteorol. Soc., 80(11), 2261–2287, doi:10.1175/1520-0477(1999)080<2261:AIUCFI>2.0.CO;2,
775 1999.

776 Ryu, Y.-H., Hodzic, A., Descombes, G., Hall, S., Minnis, P., Spangenberg, D., Ullmann, K. and
777 Madronich, S.: Improved modeling of cloudy-sky actinic flux using satellite cloud retrievals,
778 Geophys. Res. Lett., 44(3), 2016GL071892, doi:10.1002/2016GL071892, 2017.

779 Sarwar, G., Godowitch, J., Henderson, B. H., Fahey, K., Pouliot, G., Hutzell, W. T., Mathur, R.,
780 Kang, D., Goliff, W. S. and Stockwell, W. R.: A comparison of atmospheric composition using
781 the Carbon Bond and Regional Atmospheric Chemistry Mechanisms, Atmos Chem Phys, 13(19),
782 9695–9712, doi:10.5194/acp-13-9695-2013, 2013.

783 Sillman, S. and He, D.: Some theoretical results concerning O3-NOx-VOC chemistry and NOx-
784 VOC indicators, J. Geophys. Res. Atmospheres, 107(D22), 4659, doi:10.1029/2001JD001123,
785 2002.

786 Sun-Mack, S., Minnis, P., Chen, Y., Kato, S., Yi, Y., Gibson, S. C., Heck, P. W. and Winker, D.
787 M.: Regional Apparent Boundary Layer Lapse Rates Determined from CALIPSO and MODIS
788 Data for Cloud-Height Determination, J. Appl. Meteorol. Climatol., 53(4), 990–1011,
789 doi:10.1175/JAMC-D-13-081.1, 2014.

790 Tang, W., Cohan, D. S., Pour-Biazar, A., Lamsal, L. N., White, A. T., Xiao, X., Zhou, W.,
791 Henderson, B. H. and Lash, B. F.: Influence of satellite-derived photolysis rates and NOx
792 emissions on Texas ozone modeling, Atmos Chem Phys, 15(4), 1601–1619, doi:10.5194/acp-15-
793 1601-2015, 2015.

794 Tang, Y., Lee, P., Tsidulko, M., Huang, H.-C., McQueen, J. T., DiMego, G. J., Emmons, L. K.,
795 Pierce, R. B., Thompson, A. M., Lin, H.-M., Kang, D., Tong, D., Yu, S., Mathur, R., Pleim, J. E.,
796 Otte, T. L., Pouliot, G., Young, J. O., Schere, K. L., Davidson, P. M. and Stajner, I.: The impact
797 of chemical lateral boundary conditions on CMAQ predictions of tropospheric ozone over the
798 continental United States, Environ. Fluid Mech., 9(1), 43–58, doi:10.1007/s10652-008-9092-5,
799 2009.

800 Thiel, S., Ammannato, L., Bais, A., Bandy, B., Blumthaler, M., Bohn, B., Engelsen, O., Gobbi,
801 G. P., Gröbner, J., Jäkel, E., Junkermann, W., Kazadzis, S., Kift, R., Kjeldstad, B., Kouremeti, N.,
802 Kylling, A., Mayer, B., Monks, P. S., Reeves, C. E., Schallhart, B., Scheirer, R., Schmidt, S.,
803 Schmitt, R., Schreder, J., Silbernagl, R., Topaloglou, C., Thorseth, T. M., Webb, A. R.,
804 Wendisch, M. and Werle, P.: Influence of clouds on the spectral actinic flux density in the lower
805 troposphere (INSPECTRO): overview of the field campaigns, Atmos Chem Phys, 8(6), 1789–
806 1812, doi:10.5194/acp-8-1789-2008, 2008.

807 Thompson, G., Field, P. R., Rasmussen, R. M. and Hall, W. D.: Explicit Forecasts of Winter
808 Precipitation Using an Improved Bulk Microphysics Scheme. Part II: Implementation of a New
809 Snow Parameterization, Mon. Weather Rev., 136(12), 5095–5115,
810 doi:10.1175/2008MWR2387.1, 2008.

811 Toon, O. B., Maring, H., Dibb, J., Ferrare, R., Jacob, D. J., Jensen, E. J., Luo, Z. J., Mace, G. G.,
812 Pan, L. L., Pfister, L., Rosenlof, K. H., Redemann, J., Reid, J. S., Singh, H. B., Thompson, A. M.,
813 Yokelson, R., Minnis, P., Chen, G., Jucks, K. W. and Pszenny, A.: Planning, implementation,
814 and scientific goals of the Studies of Emissions and Atmospheric Composition, Clouds and

Climate Coupling by Regional Surveys (SEAC4RS) field mission, J. Geophys. Res. Atmospheres, 121(9), 2015JD024297, doi:10.1002/2015JD024297, 2016.

Travis, K. R., Jacob, D. J., Fisher, J. A., Kim, P. S., Marais, E. A., Zhu, L., Yu, K., Miller, C. C., Yantosca, R. M., Sulprizio, M. P., Thompson, A. M., Wennberg, P. O., Crounse, J. D., St. Clair, J. M., Cohen, R. C., Laughner, J. L., Dibb, J. E., Hall, S. R., Ullmann, K., Wolfe, G. M., Pollack, I. B., Peischl, J., Neuman, J. A. and Zhou, X.: Why do models overestimate surface ozone in the Southeast United States?, Atmos Chem Phys, 16(21), 13561–13577, doi:10.5194/acp-16-13561-2016, 2016.

Wiedinmyer, C., Akagi, S. K., Yokelson, R. J., Emmons, L. K., Al-Saadi, J. A., Orlando, J. J. and Soja, A. J.: The Fire INventory from NCAR (FINN): a high resolution global model to estimate the emissions from open burning, Geosci Model Dev, 4(3), 625–641, doi:10.5194/gmd-4-625-2011, 2011.

Yang, P., Hong, G., Kattawar, G. W., Minnis, P. and Hu, Y.: Uncertainties Associated With the Surface Texture of Ice Particles in Satellite-Based Retrieval of Cirrus Clouds: Part II #x2014;Effect of Particle Surface Roughness on Retrieved Cloud Optical Thickness and Effective Particle Size, IEEE Trans. Geosci. Remote Sens., 46(7), 1948–1957, doi:10.1109/TGRS.2008.916472, 2008.

Zhang, F., Bei, N., Nielsen-Gammon, J. W., Li, G., Zhang, R., Stuart, A. and Aksoy, A.: Impacts of meteorological uncertainties on ozone pollution predictability estimated through meteorological and photochemical ensemble forecasts, J. Geophys. Res. Atmospheres, 112(D4), D04304, doi:10.1029/2006JD007429, 2007.

Zhang, Y., Bocquet, M., Mallet, V., Seigneur, C. and Baklanov, A.: Real-time air quality forecasting, part II: State of the science, current research needs, and future prospects, Atmos. Environ., 60, 656–676, doi:10.1016/j.atmosenv.2012.02.041, 2012.

Table 1. Description of WRF-Chem simulations.

	Photolysis rates	PAR	Analysis Period
CNTR	WRF clouds	WRF clouds	06 UTC 11 June–12 UTC 1 October
GOES	GOES clouds	GOES clouds	06 UTC 11 June–12 UTC 1 October
EMIS_BVOC	GOES clouds	WRF clouds	06 UTC 3 July–12 UTC 13 July

874 Table 2. Contingency table for WRF simulation and GOES satellite clouds. The number of data
875 for each category is normalized by the total number of data.

		GOES Satellite	
		Cloudy	Clear
WRF simulation	Cloudy	A (hit) 24.8%	B (false alarm) 10.4%
	Clear	C (miss) 19.8%	D (correct negative) 44.9%

876
877
878
879
880
881
882
883
884
885
886

887 Table 3. Sensitivity coefficient of O_3 to JNO_2, i.e., $d\ln(O_3)/d\ln(JNO_2)$. The values of
888 $d\ln(O_3)/d\ln(JNO_2)$ for the period of 09–13 LST are averages over only CONUS EPA stations
889 that have monotonically increasing O_3 concentrations with time.

	Cloudy sky (5 < COD < 20)	Clear sky
VOC-limited	0.59	1.27
NO_X-limited	0.35	0.77

890
891
892
893
894
895
896
897
898
899
900
901
902

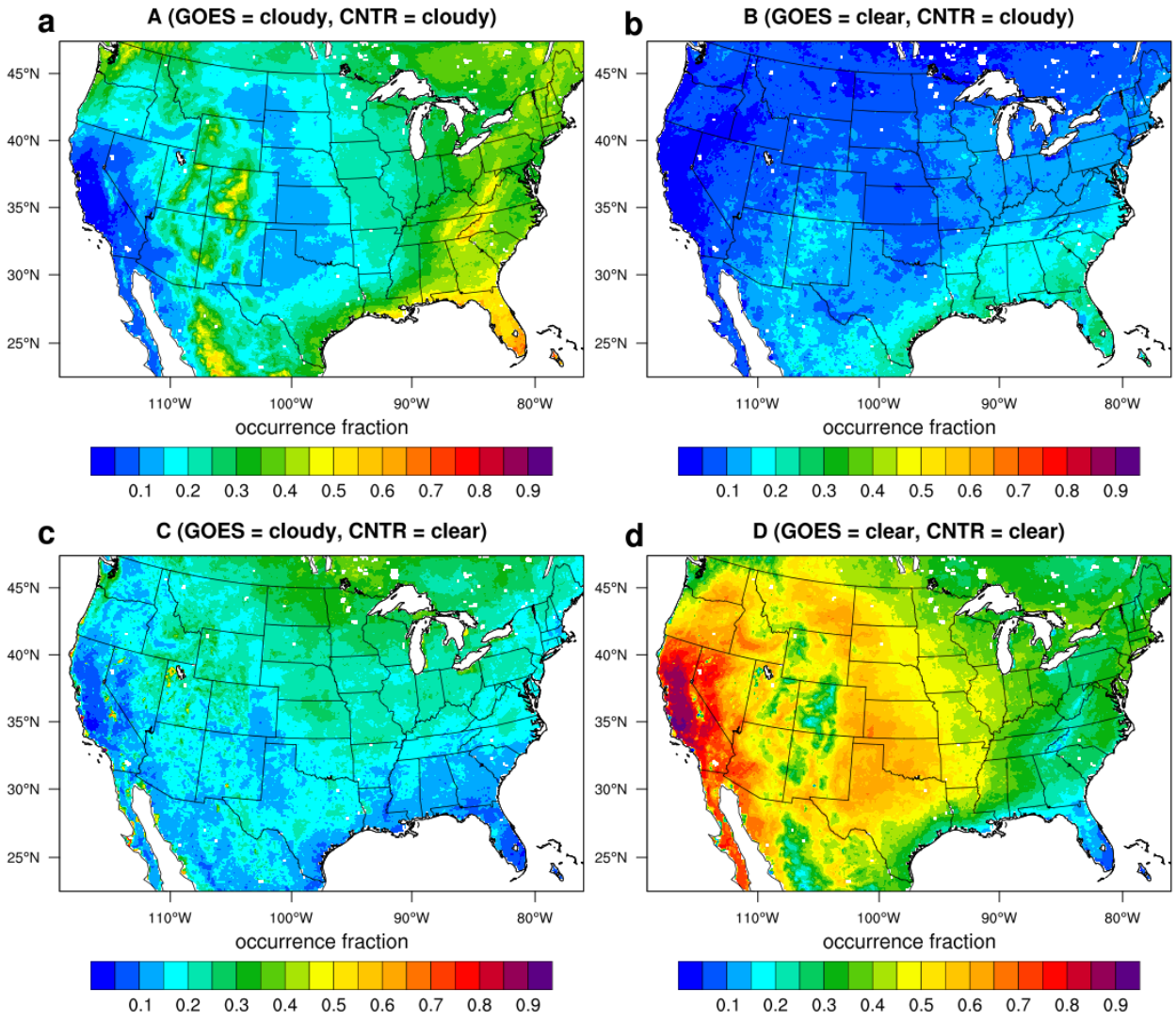

903

904 Fig. 1. Spatial distribution of each contingency category (see Table 2) between the WRF-
905 generated clouds (CNTR simulation) and SatCORPS GOES retrievals averaged over the whole
906 study period.

907

908

909

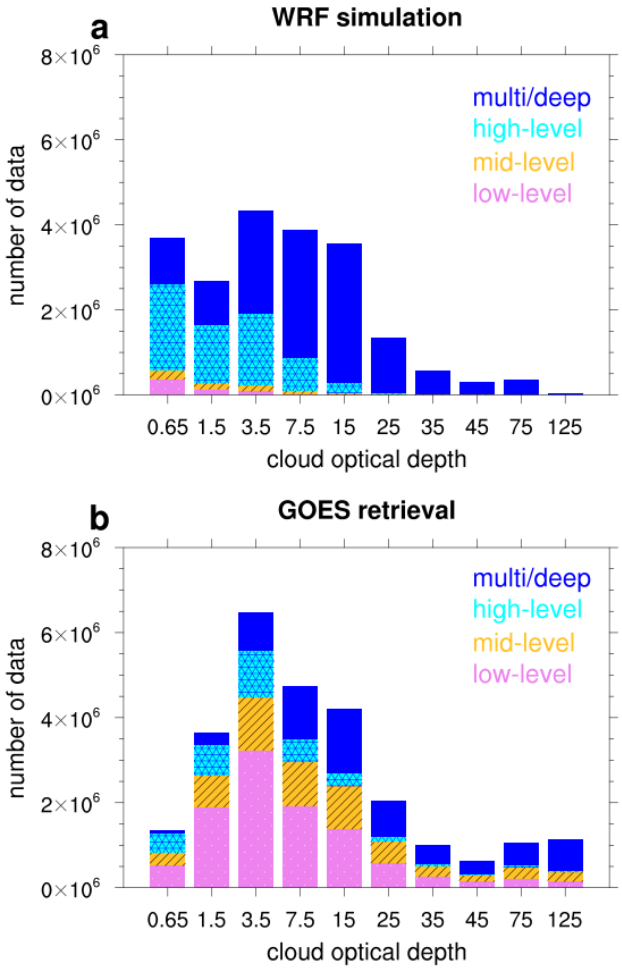

910

911 Fig. 2. Histogram of hourly cloud optical depth (COD) during the daytime (16–23 UTC) over
912 CONUS (land only) from the (a) WRF simulation (with the Morrison microphysics and the Grell
913 3-D schemes) and (b) GOES satellite retrievals. CODs on the *x*-axis represent the mean values of
914 the bins that are 0.3–1, 1–2, 2–5, 5–10, 10–20, 20–30, 30–40, 40–50, 50–100, and 100–150. For
915 a fair comparison, the multi-layered WRF clouds are not resolved into cloud layers as this
916 layering cannot be resolved by the satellite.

917

918

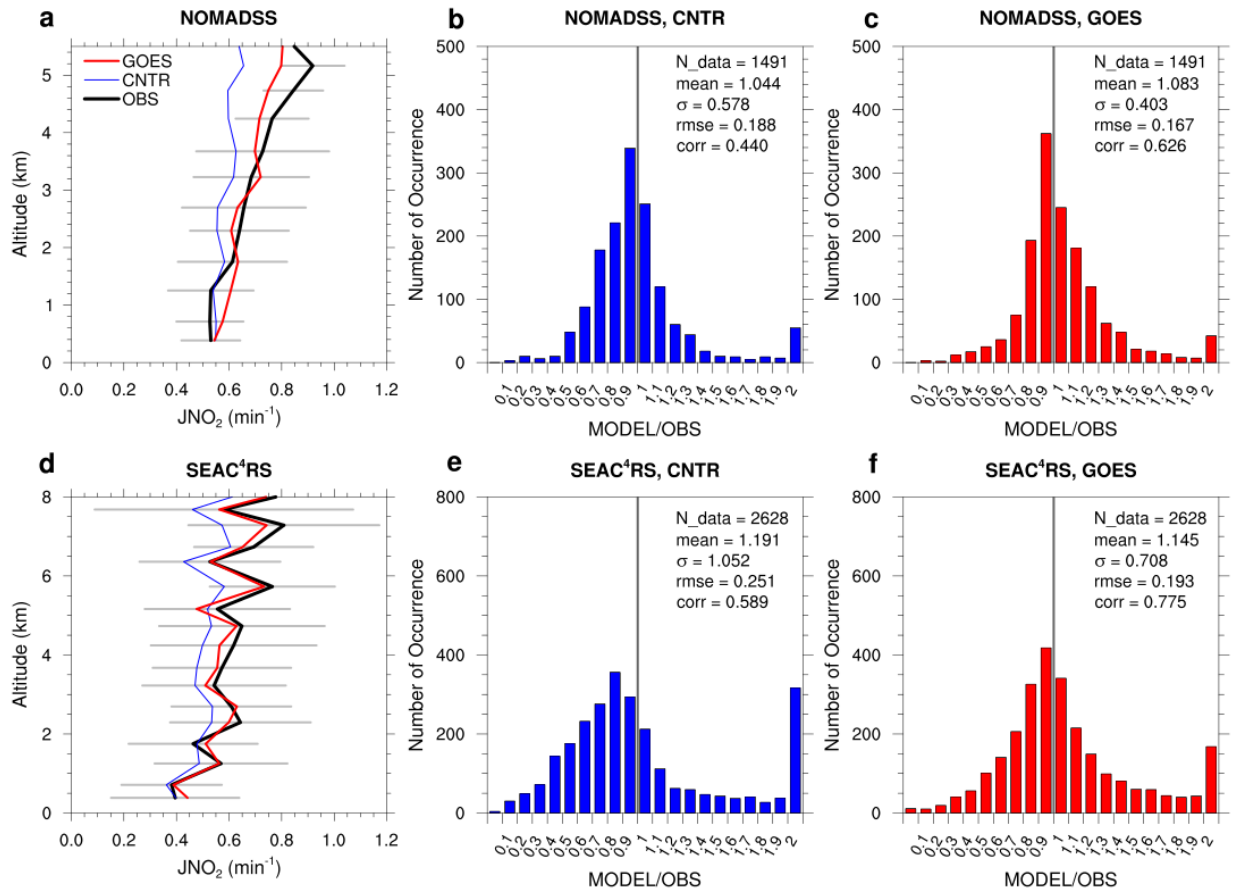

Fig. 3. Model evaluation with 16 NOMADSS flights (top row) and with 21 SEAC^{4}RS flights (bottom row). Note that only cloudy skies are considered. The comparison is performed for the averaged vertical profiles of JNO_2 for the (a) NOMADSS and (d) SEAC^{4}RS. The gray horizontal lines indicate the standard deviations from the observations. Histogram of ratio of JNO_2 simulated by the model to JNO_2 observed (b) in the CNTR simulation and (c) in the GOES simulation for the NOMADSS. (e and f) are the same as (b and c), respectively, but for the SEAC^{4}RS.

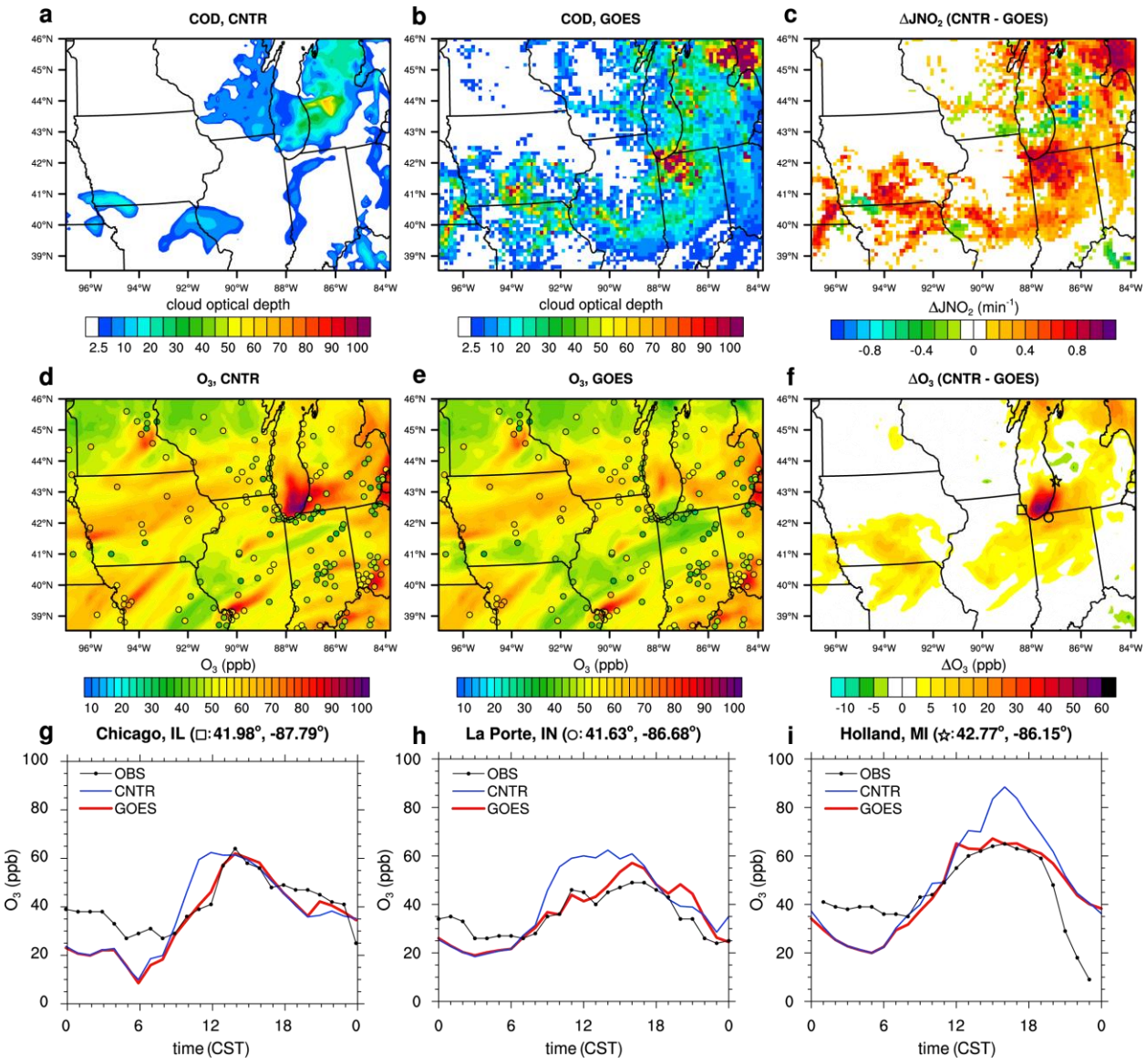

Fig. 4. Horizontal distributions of cloud optical depth at 13 ~~LST~~CST (= 19 UTC) 8 July 2013 (a) in the ~~control~~CNTR simulation and (b) in the GOES simulation. Horizontal distributions of O_3 at 13 ~~LST~~CST 8 July 2013 at the lowest model level (shaded) (d) in the ~~control~~CNTR simulation and (e) in the GOES simulation. The circles indicate EPA ozone measurements. (c and f) Difference in JNO_2 and O_3, respectively, between the simulations (i.e., ~~control~~CNTR simulation minus GOES simulation). (g, h, and i) Time series of O_3 at the square (Chicago, IL), circle (La Porte, IN), and star (Holland, MI) that are marked in (f), respectively.

937

938

939

940

941

942

943

944

945

946

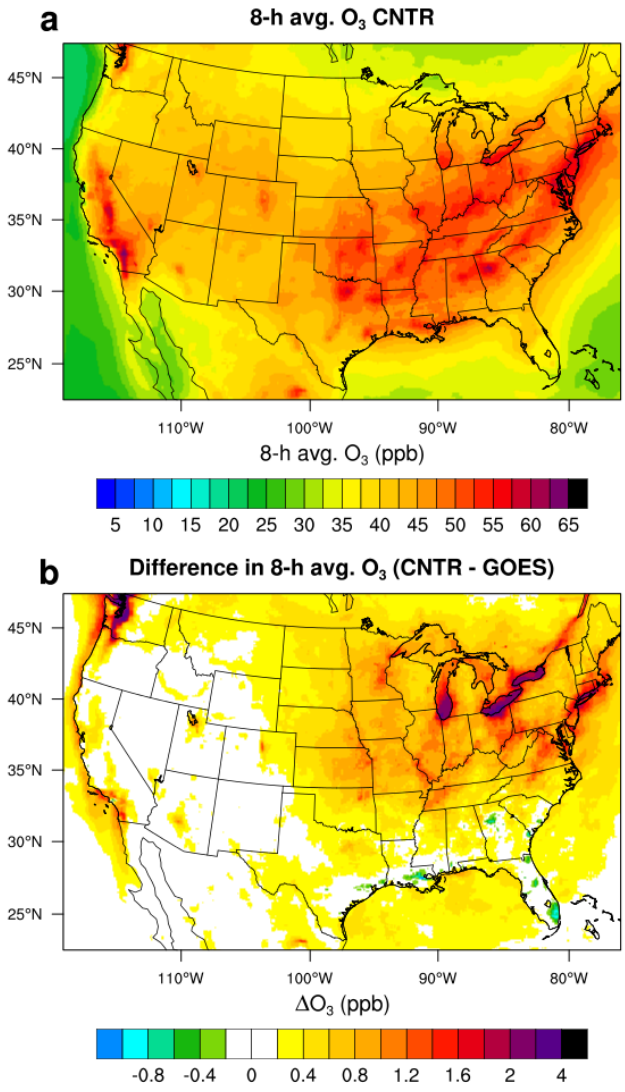
a
8-h avg. O3 CNTR
45°N
40°N
35°N
30°N
25°N
110°W
100°W
90°W
80°W
8-h avg. O3 (ppb)
5 10 15 20 25 30 35 40 45 50 55 60 65
b
Difference in 8-h avg. O3 (CNTR - GOES)
45°N
40°N
35°N
30°N
25°N
110°W
100°W
90°W
80°W
ΔO3 (ppb)
-0.8 -0.4 0 0.4 0.8 1.2 1.6 2 4

947

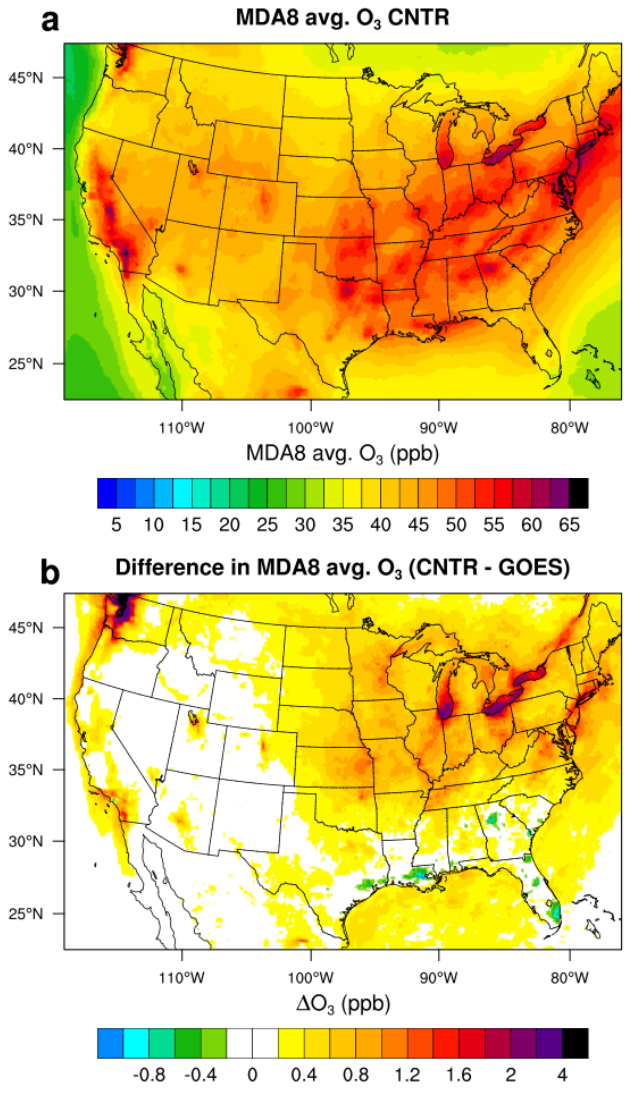

Fig. 5. (a) Spatial distribution of maximum daily 8-h average O_3 (MDA8 O_3) at the lowest model level averaged over the whole analysis period in the CNTR simulation. (b) Difference in ~~8-h~~ ~~average~~MDA8 O_3 at the lowest model level between the control and GOES simulations (i.e., CNTR minus GOES).

955

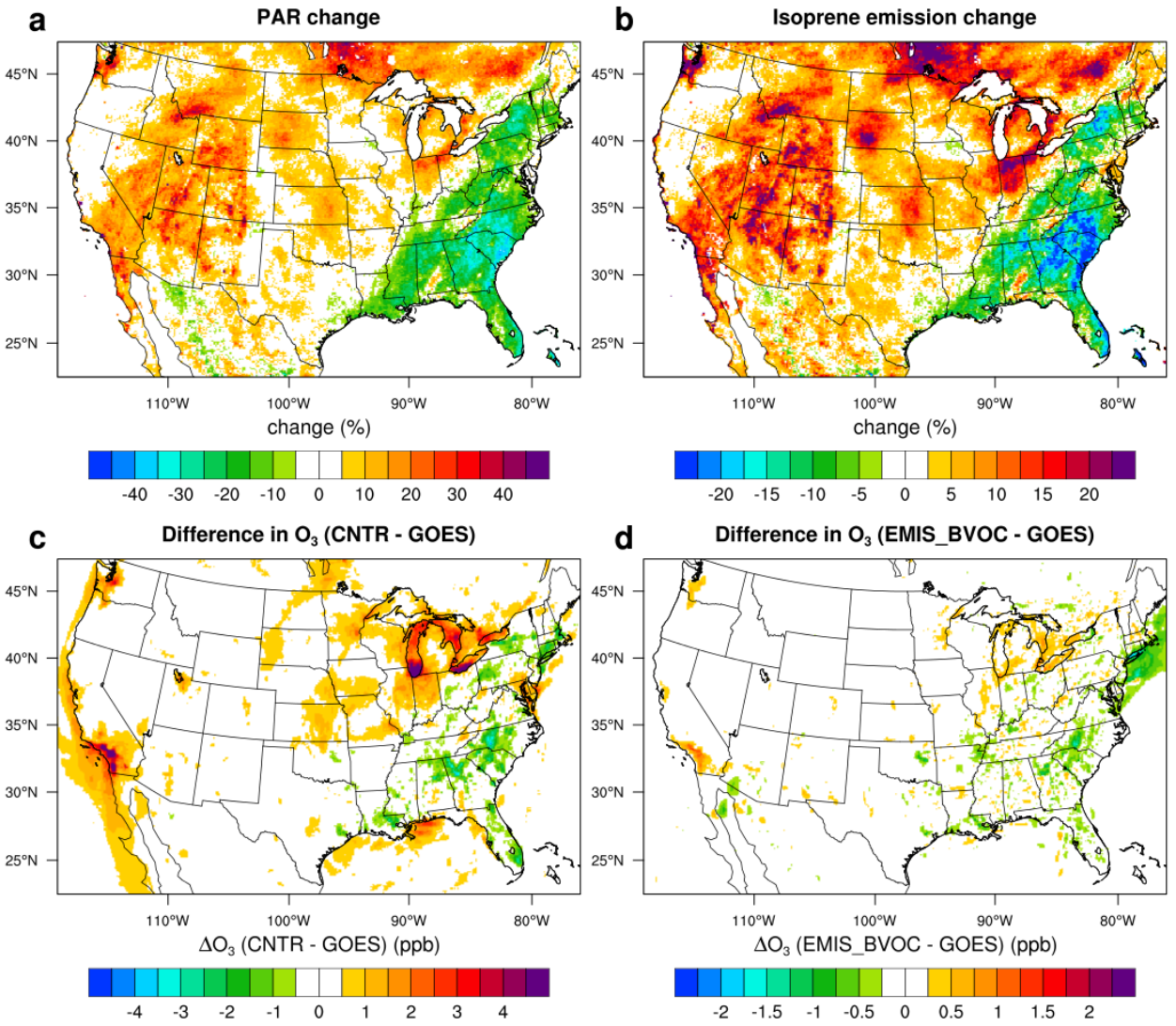
a
PAR change
45°N
40°N
35°N
30°N
25°N
110°W
100°W
90°W
80°W
change (%)
-40 -30 -20 -10 0 10 20 30 40
b
Isoprene emission change
45°N
40°N
35°N
30°N
25°N
110°W
100°W
90°W
80°W
change (%)
-20 -15 -10 -5 0 5 10 15 20
c
Difference in O_3 (CNTR - GOES)
45°N
40°N
35°N
30°N
25°N
110°W
100°W
90°W
80°W
ΔO_3 (CNTR - GOES) (ppb)
-4 -3 -2 -1 0 1 2 3 4
d
Difference in O_3 (EMIS_BVOC - GOES)
45°N
40°N
35°N
30°N
25°N
110°W
100°W
90°W
80°W
ΔO_3 (EMIS_BVOC - GOES) (ppb)
-2 -1.5 -1 -0.5 0 0.5 1 1.5 2

956

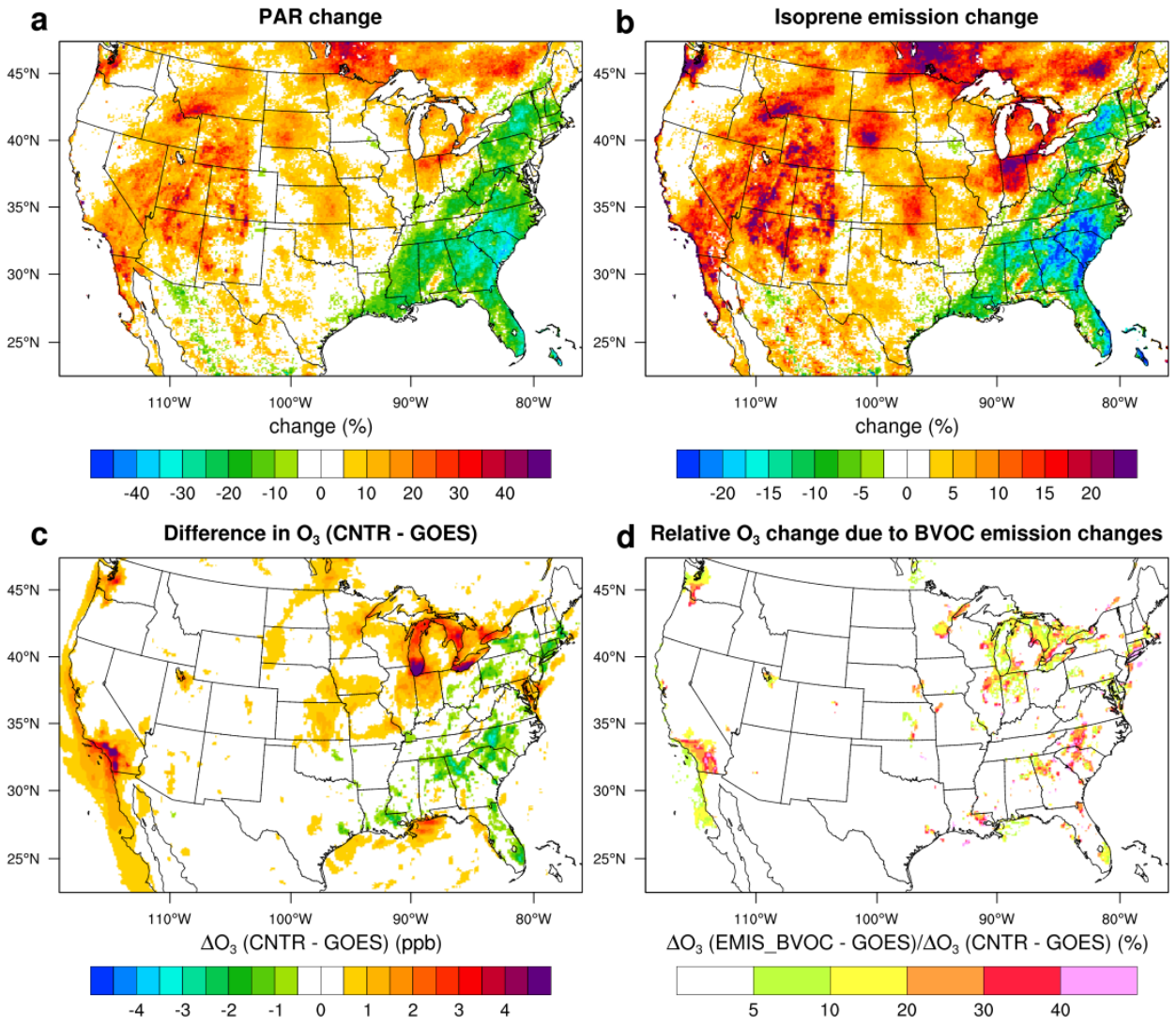

957

958 Fig. 6. Spatial distributions of (a) PAR change and (b) isoprene emission change from biogenic
959 sources between EMIS_BVOC and GOES simulations, (EMIS_BVOC–GOES)/GOES, averaged
960 over the period of 3–12 July 2013. (c) Difference in O_3 ~~(c)~~ between the CNTR and GOES
961 simulations ~~and.~~ (d) Ratio of O_3 difference between EMIS_BVOC and GOES simulations~~.~~ to O_3
962 difference between CNTR and GOES simulations, i.e., ΔO_3(EMIS_BVOC–GOES)/ΔO_3 (CNTR–
963 GOES). Note that the grids that have considerable O_3 difference between CNTR and GOES
964 simulations (> 1 ppb) are depicted in (d).

965

966

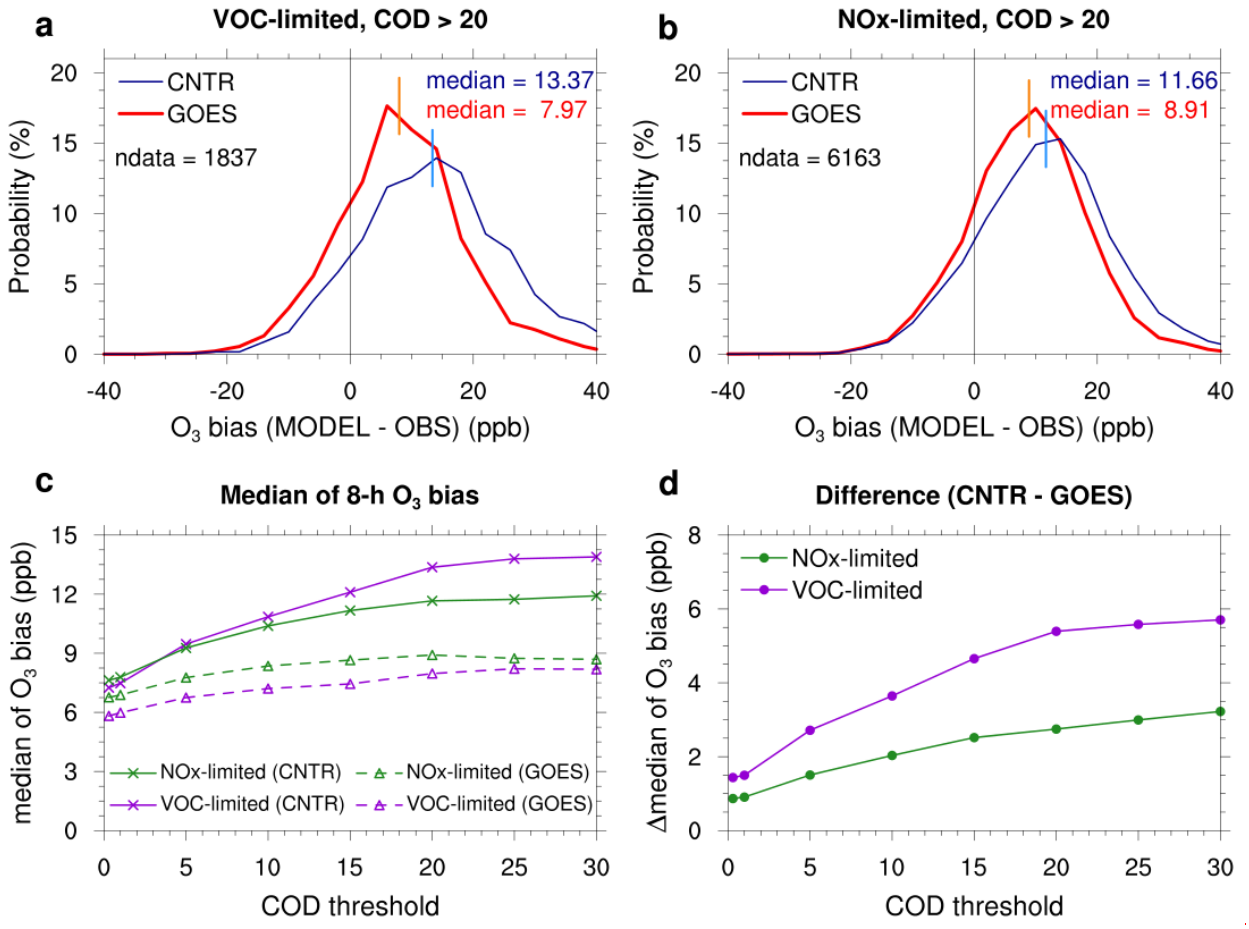
a
VOC-limited, COD > 20
CNTR
GOES
ndata = 1837
median = 13.37
median = 7.97
Probability (%)
O3 bias (MODEL - OBS) (ppb)
b
NOx-limited, COD > 20
CNTR
GOES
ndata = 6163
median = 11.66
median = 8.91
Probability (%)
O3 bias (MODEL - OBS) (ppb)
c
Median of 8-h O3 bias
median of O3 bias (ppb)
NOx-limited (CNTR)
NOx-limited (GOES)
VOC-limited (CNTR)
VOC-limited (GOES)
COD threshold
d
Difference (CNTR - GOES)
Δmedian of O3 bias (ppb)
NOx-limited
VOC-limited
COD threshold

967

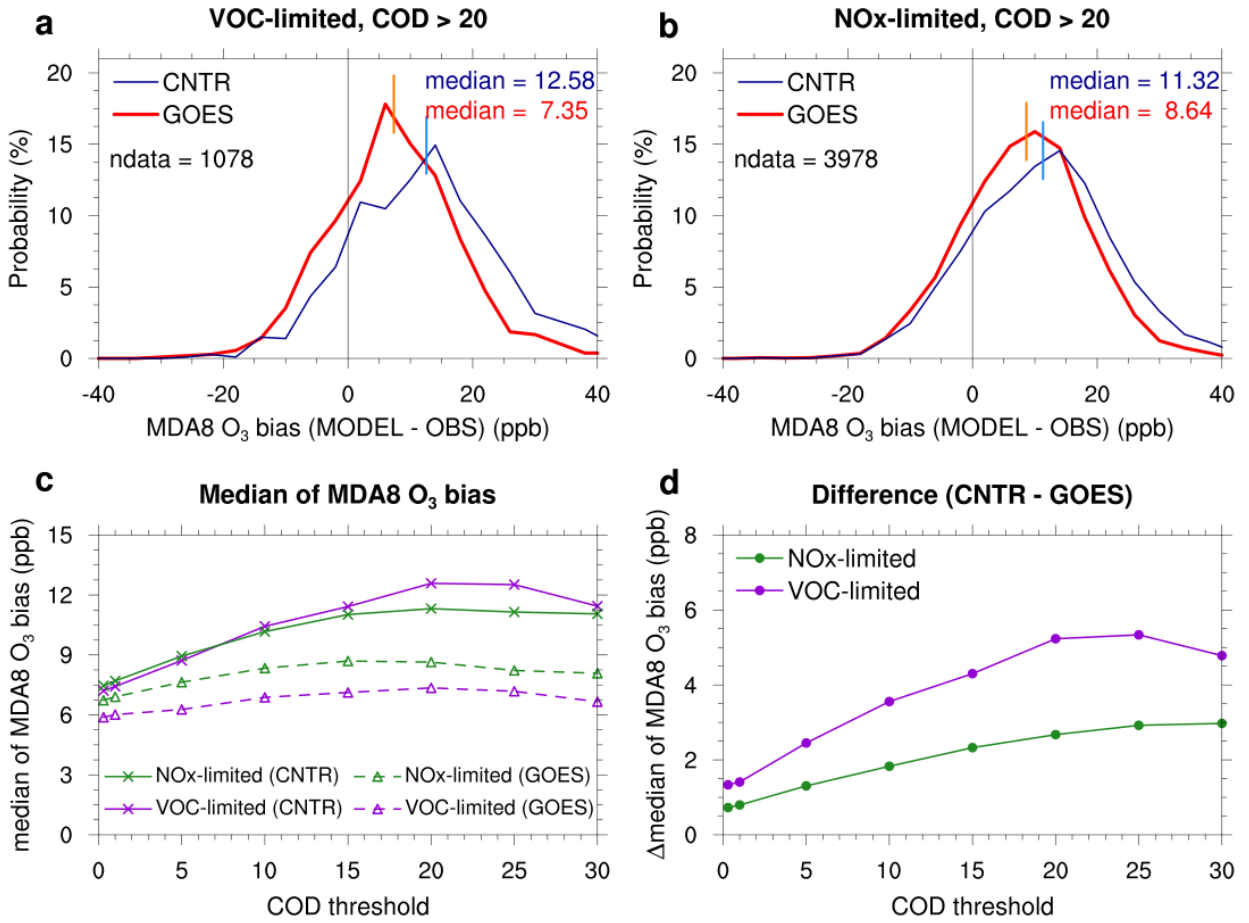

Fig. 7. (a) Probability density function of ~~8-h~~maximum daily 8-h average (MDA8) O_3 bias (model value minus observation value) for VOC-limited regime under cloudy sky conditions defined with COD threshold of 20. (b) Same as (a), but for NO_X-limited regime. (c) Median values of ~~8-h~~MDA8 O_3 bias with respect to COD threshold in the CNTR simulation (solid lines with cross marks) and in the GOES simulation (dashed line with triangles) for VOC-limited (purple color) and NO_X-limited regimes (green color). (d) Difference in median values of ~~8-h~~MDA8 O_3 bias between the two simulations with respect to COD threshold (i.e., CNTR minus GOES).

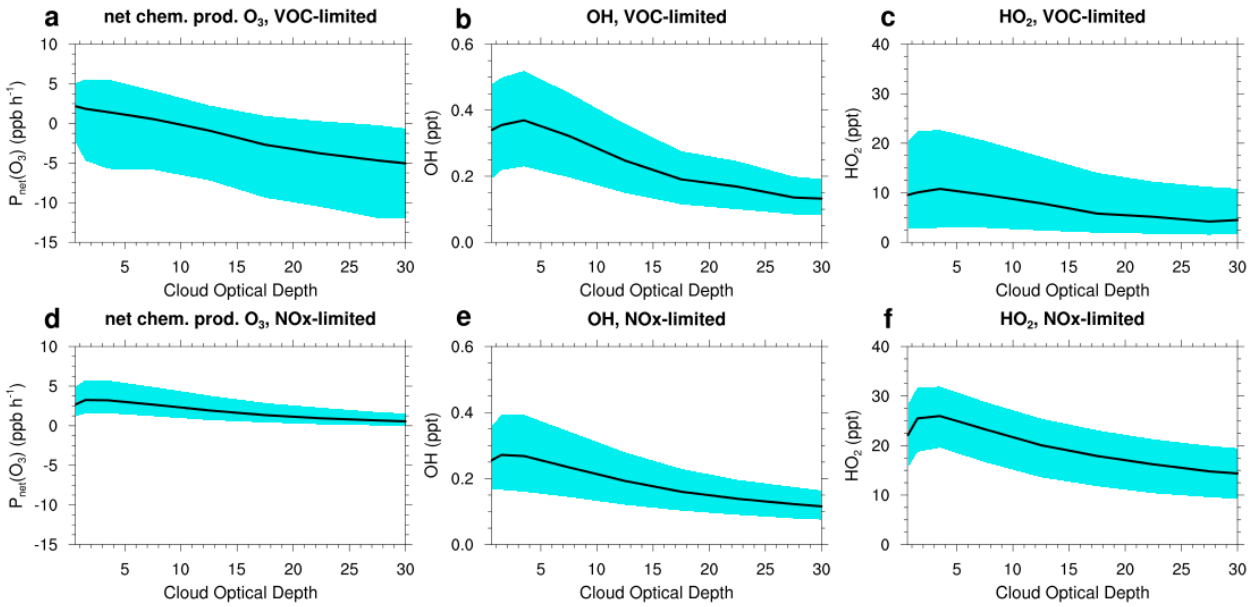

Fig. 8. (a) Net chemical production of O_3, (b) OH concentration, and (c) HO_2 concentration with variations of cloud optical depth for VOC-limited regime. The black line indicates the median and cyan shading indicates the 25 and 75 percentiles. Similar variables are shown for the NO_X-limited regimes (d, e, and f).

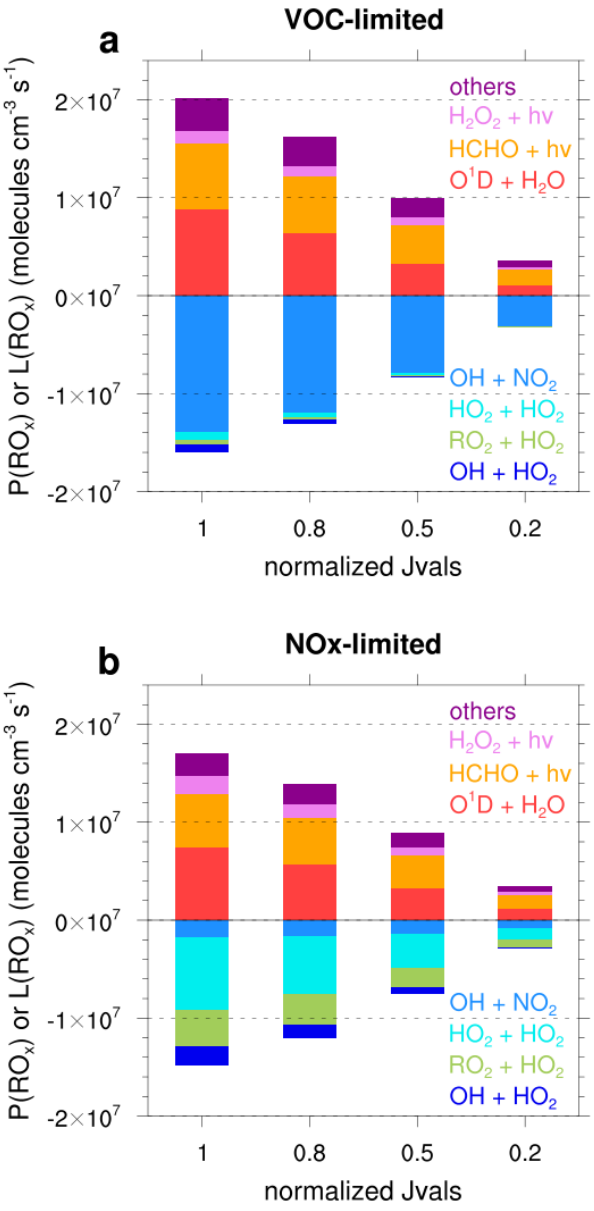

Fig. 9. Results of box modeling for production and loss rates of ROx (= OH + HO_2 + RO_2) radicals. "Others" in the legend indicates the photolysis of VOCs and reactions between alkenes and O_3. The value of 1 of normalized Jvals on *x*-axis indicates the photolysis rates for clear sky conditions.

996